Production and functionalization of cobalt nanofoams for energy storage

Naureen Khanam

Thesis to obtain the Master of Science Degree in

Energy Engineering and Management

Supervisors: Prof. Maria de Fátima Grilo da Costa Montemor
Prof. Maria Teresa Oliveira de Moura e Silva

Examination Committee

Chairperson: Duarte de Mesquita e Sousa
Supervisor: Prof. Maria Teresa Oliveira de Moura e Silva
Members of the Committee: Prof. Raquel Alexandra Galamba Duarte
Dr. Alberto Adán Más

October 2019

I declare that this document is an original work of my own authorship and that it fulfils all the requirements of the Code of Conduct and Good Practices of the *Universidade de Lisboa*.

Acknowledgements

All praise to the Almighty, the Most Merciful.

I would like to express gratitude to my supervisors Professor Fátima Montemor and Professor Maria Terresa Moura e Silva for their continuous guidance, advices and support during this work.

My heartful gratitude to Dr. Alberto Adán Más for his support and all the endeavours to teach me everything from zero.

I would like to thank EIT KIC InnoEnergy for providing scholarship under CFAFE program for my master study.

This research work was developed under IDI&CA/SuperStore 0712045/ISEL project funded by Instituto Politécnico de Lisboa. I would like to thank this institution for offering me the scientific initiation fellowship under this project.

I appreciate all the support of my colleagues for their help, support and kindness throughout this master study in two different countries.

Finally, respect and love for my family and friends who helped keeping my moral spirit high during this journey from thousand miles apart.

Abstract

Highly porous surface areas with high capacitive and good conductive response are important requirements for materials to be used as supercapacitor electrodes. Metallic cobalt has the advantage of high conductivity and cobalt oxides possess high pseudocapacitive response. Cobalt nanofoam was produced on stainless steel substrate by the dynamic hydrogen bubble template (DHBT) method to obtain honeycomb like morphology with cauliflower agglomerates. Cyclic voltammograms of the Co nanofoam indicated a combination of pseudocapacitive and intercalation type response with partial redox wave like signature and $Co(OH)_2$ was seen as the electrochemically active phase in 1 M KOH. Nanofoams were treated by thermal, chemical and electrochemical oxidation processes for improving the electrochemical response. Co nanofoam, chemically oxidized with 5% H_2O_2 for 24 hours exhibited faradaic response with specific capacity of 26 mAh g^{-1} at 1Ag^{-1}. An asymmetric electrochemical cell fabricated with chemically treated Co nanofoam as positive and carbon as negative electrode, showed pseudocapacitive response with 34.6 Fg^{-1} specific capacitance at 0.1 Ag^{-1}. The cell exhibited specific energy of 7.8 Wh kg^{-1} at a power density of 63.6 kW kg^{-1} and the value did not show any meaningful decrease at a power density of 1288 kW kg^{-1}. The cell stability was measured during 2000 cycles of galvanostatic charge discharge and only 10% of capacitance loss was observed. Given the potential window performance, Co nanofoam, chemically treated with 5% H_2O_2 for 24 hours showed good potential as the positive electrode in asymmetric supercapacitors.

Keywords

Cobalt nanofoam, cobalt oxides, DHBT electrodeposition, supercapacitors, energy storage.

Resumo

Áreas superficiais elevadas e porosidade controlada são a chave para se conseguir boa resposta capacitiva de materiais utilizados como elétrodos de supercondensadores. O cobalto metálico tem uma elevada condutividade e os respetivos óxidos possuem uma boa resposta pseudocapacitiva. Neste trabalho produziu-se uma nano-espuma de cobalto por electrodeposição num substrato de aço inoxidável, através do método dinâmico de bolha de hidrogénio. Os voltamogramas revelaram uma resposta eletroquímica mista envolvendo processos pseudocapacitivos e de intercalação, além de evidenciarem o $Co(OH)_2$ como a fase electroquimicamente ativa em KOH 1 M. As nano-espumas foram submetidas a tratamentos térmicos e de oxidação química ou electroquímica, de modo a melhorar a sua resposta em termos a capacidade de armazenamento de carga. Nano-espumas de cobalto, oxidadas quimicamente por imersão em 5% H_2O_2 durante 24h, apresentaram uma resposta farádica e valores de capacidade específica de 26.1 mAh g^{-1}. Foi desenvolvido um supercondensador assimétrico utilizando a nano-espuma de cobalto oxidada como elétrodo positivo e carbono ativado como elétrodo negativo. A célula evidenciou uma resposta pseudocapacitiva apresentando uma capacidade específica de 34.6 Fg^{-1} a uma densidade de corrente de 0.1 Ag^{-1}. Esta célula manteve uma energia específica de 7.8 Wh kg^{-1} para densidades de potência compreendidas entre 63.6 kW kg^{-1} e 1288 kW kg^{-1}. A estabilidade do dispositivo foi avaliada através da imposição de 2000 ciclos consecutivos de carga-descarga, verificando-se uma perda de apenas 10% no valor da capacidade. Considerando a resposta observada, a nano-espuma de cobalto tratada quimicamente com H_2O_2 5% durante 24 horas tem potencial enquanto elétrodo positivo.

Palavras-chave

Nano-espumas de cobalto, óxidos cobalto, electrodeposição, supercondensadores, armazenamento de energia

Table of Contents

List of Figures

List of Tables

List of Acronyms

EDLC	Electrochemical double layer capacitor
SCE	Saturated calomel electrode
CV	Cyclic voltammetry
GCD	Galvanostatic charge discharge
DHBT	Dynamic hydrogen bubble template
SEM	Scanning Electron Microscopy
EDS	Electron Diffraction Spectroscopy
XRD	X-ray Diffraction
EIS	Electrochemical Impedance Spectroscopy

List of Variables

Variable	Name	Unit
C	Capacitance	F
A	Surface area	m^2
d	Thickness	m
I	Current	A
m	Mass	g or kg
t	Time	sec or hour
t_c	Charging time	sec
t_d	Discharging time	sec
η	Coulombic efficiency	%
ΔV	Potential range	V
ω	Frequency	Hz
Z	Impedance	Ohm
E	Specific energy	$Wh\ kg^{-1}$
P	Specific power	$W\ kg^{-1}$

Chapter 1

Introduction

Energy transition from fossil fuels to renewable sources demand rapid action in the area of energy storage. Among different energy storage systems, supercapacitors are being investigated for their better power density compared to rechargeable batteries. In this research, the potential of cobalt nanofoams as electrode materials for supercapacitors has been investigated. The goal of this research was the electrodeposition of cobalt foam with controlled morphology and its structural functionalization to obtain cobalt oxides that may be used in energy storage. In this chapter, an overview of supercapacitor as energy storage system, the state of art of supercapacitor electrode materials, nanofoam production process and the properties of cobalt metal and cobalt oxides are presented.

1.1 Overview

Global demand of energy has increased tremendously in last few decades due to the increased population, economic growth as well as expectation of better life standard among the world population[1]. Estimated energy consumption increase is about one third by 2040, large portion is because of the fast-growing emerging economies[1]. To cope with the increasing energy demand, new alternative sources of energy are being evaluated. In addition to the search of new energy sources, climate change and CO_2 emission problems have turned the focus of primary energy sources from fossil fuels to greener energy sources. On grounds of the intermittent nature of renewable energy, in this modern era of energy transition, efficient and economically feasible energy storage systems are being investigated.

Depending on the form of initial and final energy to be stored, Electricity Energy Storage (Power to Power), Thermal Energy Storage (Power to Thermal) and Chemical Energy Storage (Power to Gas/ Power to Liquid) are the basic classification of energy storage sytems[2]. Electricity Energy Storage can be sub grouped as (i)*Mechanical Energy Storage* where the energy is stored as kinetic or potential energy, (ii)*Electrochemical Energy Storage* where electrochemical reactions store electricity and (iii)*Electrical Energy Storage* systems that use electrical potential for the storage purpose by creating electrostatic potential or electromagnetic potential[2]. Among all the different forms of energy storage systems, Electrochemical Energy Storage (EES) technologies together with materials development, have been playing leading and promising roles to tackle the challenges of global energy demand[3]. Novel materials and technological innovations based on different electrochemical reactions that lead to increased capacitance/capacity are being sought and used to develop rechargeable batteries, because of their high energy density, and supercapacitors, for high power density and long cycle life[3].

Supercapacitors, also known as Electrochemical capacitors are a subclass of capacitors. Capacitors can be divided as Electrostatic capacitors, Electrolytic capacitors and Electrochemical capacitors. First successful Electrochemical capacitor was made by Robert A. Rightmire, a chemist at the Standard Oil Company of Ohio (SOHIO) in 1960's and considered as the inventor of supercapacitor. The commercial production of supercapacitor started in 1978 by NEC under licence from SOHIO. Supercapacitors were previously used only in back-up power devices for volatile clock chips and complementary metal-oxide-semiconductor (CMOS) computer memories. The voltage and capacitance scale were very small initially that has been improved throughout the past three decades. Supercapacitor applications are now ranging from milli Farad to devices rated at hundreds of thousands of Farads[4]. Because of the improvement in capacitance, they are now being used in distributed power generation systems, industrial actuator power sources, electric vehicles and hybrid vehicles[4].

1.2 Comparison of supercapacitors with other energy storage systems

Supercapacitors are devices capable of managing hundred to thousand times higher power density but about 3-30 times lower energy storage capacity compared to batteries, that give supercapacitors preference in power intensive applications with lower energy density required[5]. Supercapacitors have lower power density when compared to capacitors, but can go up to 10 $kWkg^{-1}$, nonetheless, their specific energy is around a hundred times greater. Charge-discharge time for supercapacitors range from few seconds to minutes which is a great advantage for energy recovery systems. The Ragone plot in FigureFigure 1.1 demonstrates the comparison among different electrochemical energy storage systems in terms of power density and energy density.

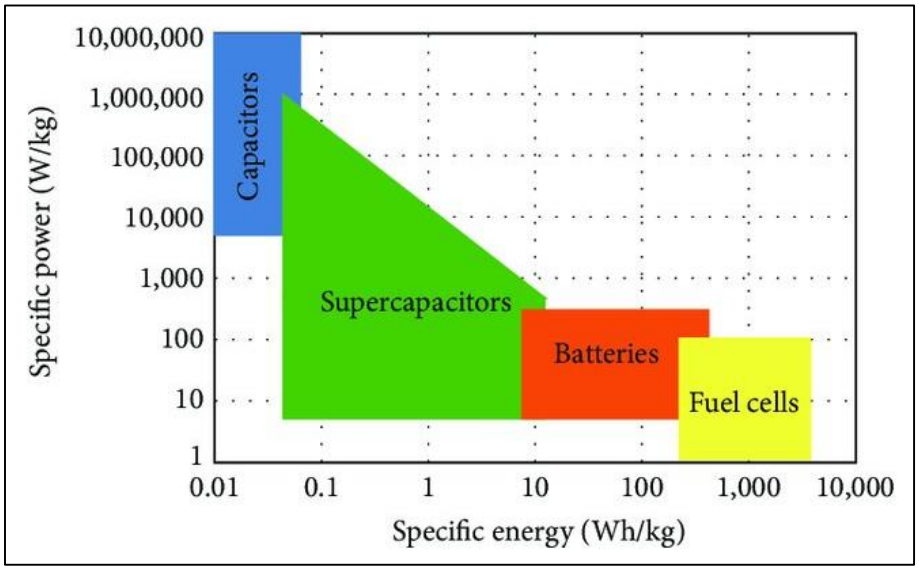

Figure 1.1 Ragone plot of different electrochemical energy storage systems[6]

Another advantage of supercapacitor over battery is the cycle life, which depends on their specific charge storage mechanism. Supercapacitors store energy at the electrode surface in the form of electrical double layers by a physical adsorption charge mechanism. This leverage supercapacitors lifetime over batteries which store energy by means of quasi-reversible chemical reactions in the bulk of the electrode, limiting the cycle life to the scale of few thousands of cycles. For supercapacitors, the electrostatic charge storage mechanism does not change the volume of electrodes, while redox reactions in batteries includes irreversible reactions, parasitic reactions causing volume gradients in the active material during charge discharge cycles. Table 1.1 & Table 1.2 compares key properties of batteries, supercapacitors and capacitors.

The performance of supercapacitor depends largely on the electrode surface/electrolyte interface. There has been extensive research about supercapacitor electrode materials and the improvement of the surface of the electrode throughout past decades[7]. Considering all the advantages and flaws, supercapacitors still need to be improved as energy storage system for higher efficiency and more research shall be done to meet the requirements of practical applications.

Table 1.1 Comparison of Supercapacitor with other Electrochemical Energy Storage Systems[5]

Characteristics	*Capacitor*	*Supercapacitor*	*Battery*
Specific Energy (Wh kg^{-1})	< 0.1	1-10	10-100
Specific Power (W kg^{-1})	>> 10000	500-10000	<10000
Charge time	10^{-6} to 10^{-3} s	sec to min	1 to 5 h
Discharge time	10^{-6} to 10^{-3} s	sec to min	0.3 to 3 h
Coulombic efficiency (%)	~100	85-98	70-85
Cycle	~Infinite	10000 to > 500000	~1000 to 5000

Table 1.2 Comparison between Batteries and Supercapacitors[5]

Comparison Parameter	*Supercapacitor*	*Battery*
Storage mechanism	Physical	Chemical
Power limitations	Electrolyte conductivity	Reaction kinetics, mass transport
Energy storage	Limited (surface area)	High (bulk)
Charge rate	High, same as discharge	Mass transport limited
Cycle life limitations	Side reactions	Mechanical stability, chemical reversibility, side reactions

1.3 Supercapacitor classification

A supercapacitor cell is comprised of one positive and one negative electrode separated by a separator and an electrolyte. The separator is immersed in the electrolyte and prevents any electrical contact between the electrodes allowing ionic conduction. The electrolyte should have high ionic permeability but must also be electrically resistive for the better performance of the cell.

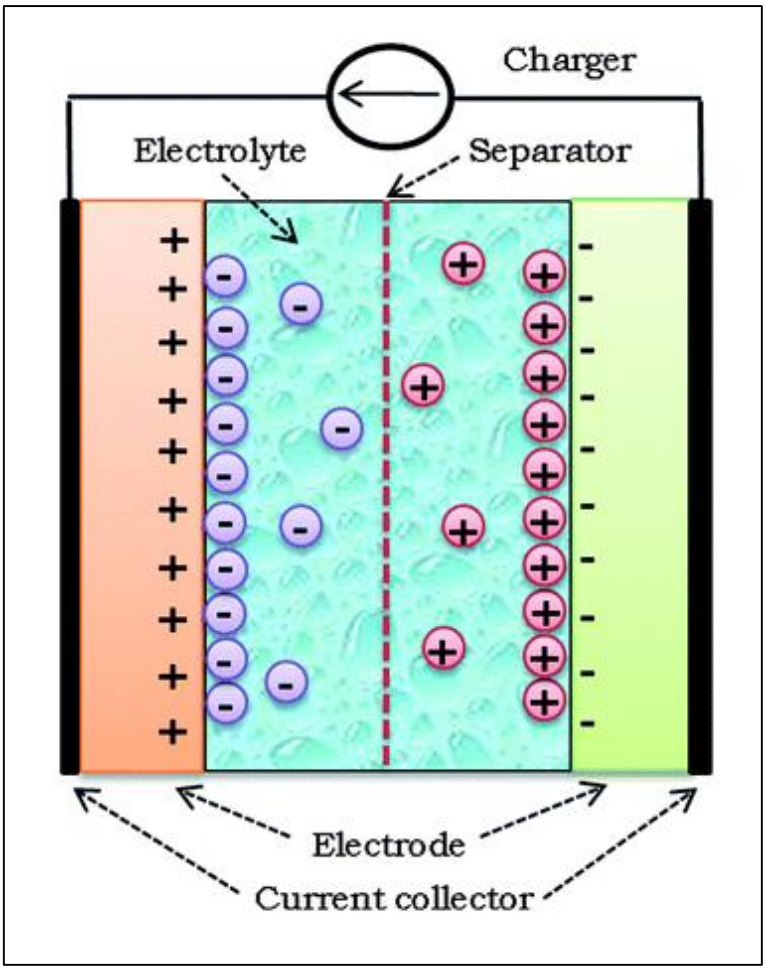

Figure 1.2 Schematic diagram of a supercapacitor cell [8].

Supercapacitors can be classified as symmetric, where both positive and negative electrodes are the same material and asymmetric, where the electrodes are made of different materials. Depending on the charge storage mechanism, supercapacitors can be classified mainly as Electrical Double Layer Capacitors (EDLCs) and Pseudocapacitors, also called redox supercapacitors. Details of the charge storage mechanism of these supercapacitors are discussed in the following sections.

1.3.1 Electrochemical double layer capacitors (EDLCs)

EDLCs mainly use non-faradaic mechanism to store energy at the electrode surface. The ions from the electrolytes are reversibly adsorbed on the electrode active material. High specific surface area is an important requirement of ELDC electrode which ensures higher capacitance. Carbon materials were used generally in EDLCs because of their high active surface area, high chemical and mechanical stability and excellent electrical conductivity. The demand of EDLCs has increased throughout the time and new applications in transportation and renewable energy storage systems have strengthened the research related to this concept[9].

The electrical double layer forms when a charged material is immersed in a liquid electrolyte. Balancing

counter charge of the charged surface of the material appears in the electrolyte surface. The interaction between the charged surface of the material and the electrolyte has been explained by several models. The simplest model is the Helmholtz model. According to this model the charge in the conductive material are neutralized by the counter charge in the electrolyte.

An updated model is given by *Gouy and Chapman*, who suggested that the same number of opposite ionic charges appear in the electrolyte, but instead of being closely attached to the conductive material, they form a diffuse layer, as seen in FigureFigure 1.3.(b). *Stern and Geary*, combined both previous models, suggesting that there is an internal Stern layer (i.e. Helmholtz layer) of specifically adsorbed ions and an outer diffuse layer (i.e. Gouy-Chapman layer) of non-specifically adsorbed counter charge[5]. The electric double layer models are shown on Figure 1.3

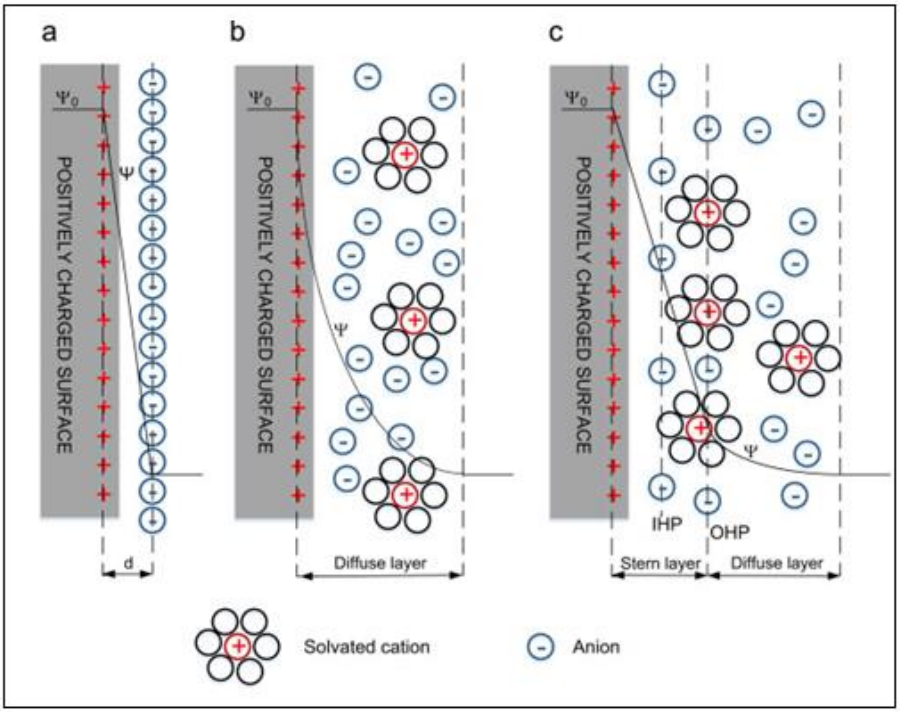

Figure 1.3 Electric double layer models, (a) Helmholtz model, (b) Gouy–Chapman model, and (c) Stern and Geary model [5]

Helmholtz described the double layer capacitance as the result from the charge separation due to polarization at the electrode electrolyte surface, according to equation 1.1:

$$C = \frac{\varepsilon_r \, \varepsilon_0 \, A}{d} \qquad (1.1)$$

where, ε_r is the dielectric constant of electrolyte, ε_0 is the dielectric constant of vacuum with a value of 8.85×10^{-12} Fm^{-1}, A is the surface area of the electrode and d is the effective thickness of the double layer (charge separation distance)[10].

Depending on the electrolytes used, double layer capacitance is typically between 5 to 20 μF cm^{-2} [9]

1.3.2 Pseudocapacitors

Pseudocapacitors store energy via faradaic mechanisms, where fast and highly reversible redox reactions occur at the active material surface for the storage purpose. Pseudocapacitors possess higher specific capacitance and higher energy density compared to EDLCs[7]. RuO_2 has been in focus as a pseudocapacitive material for past three decades because it is highly conductive and has different oxidation states[10].

The electrical response of pseudocapacitive materials are ideally same as the EDLCs, i.e. the oxidation state changes with the voltage proportionally, leading to a proportionality constant denoted as capacitance[5]. Pseudocapacitance can be intrinsic or extrinsic. Intrinsic materials show pseudocapacitive response in a wide range of size and morphologies. On the other hand, the response of extrinsic pseudocapactive materials are only present under nanosized conditions, while in the bulk, the same material shows faradaic dominated response. Pseudocapacitive materials exhibit different charge storage mechanisms like underpotential deposition, intercalation pseudocapacitance or redox reactions of the transition metals[5]. These are exemplified in Figure 1.4.

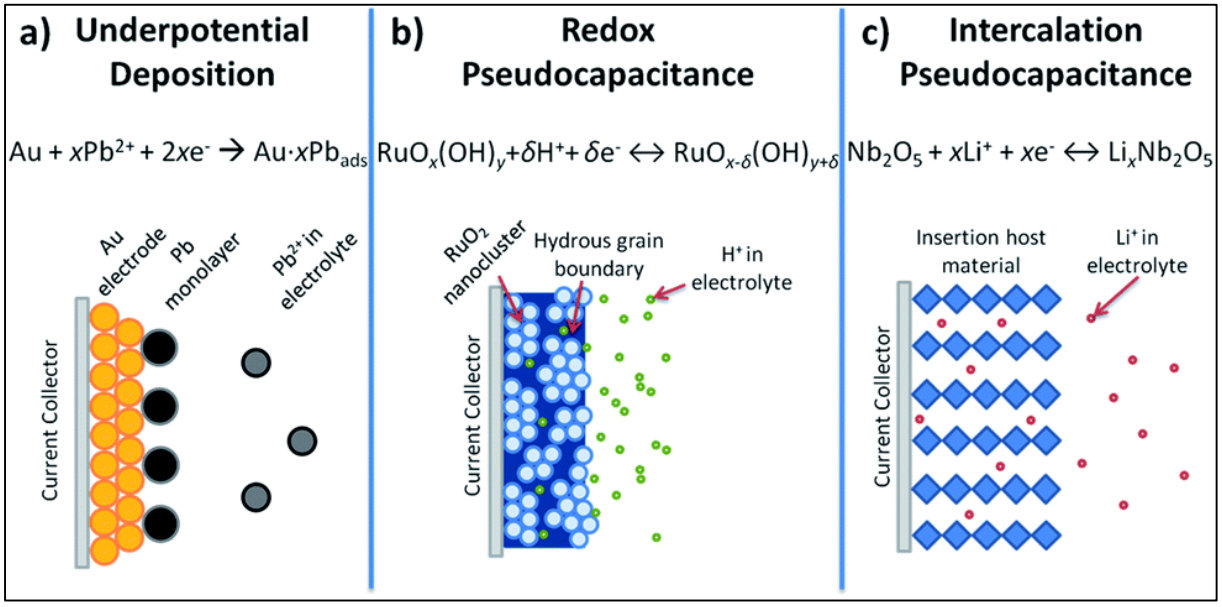

Figure 1.4 Different types of reversible redox mechanisms that give rise to the pseudocapacitance: (a) underpotential deposition, (b) redox pseudocapacitance, and (c) intercalation pseudocapacitance [11].

1.4 Materials of supercapacitors

Performance of supercapacitors largely depend on the electrode materials. Pursuit of new materials and improvement of the performance of the existing materials have been interesting topics among the researchers. The capacitance of supercapacitors depends heavily but not linearly on the specific surface area of the electrode. The reason is that, the whole surface area is not always electrochemically active

while in contact with the electrolyte. So electrochemical active surface area would be a more appropriate notation that is important requirement for materials to be used as supercapacitor electrodes[12].

In general, the electrode materials can be classified as carbon-based electrodes, conducting polymers and metal oxides.

1.4.1 Carbon

Carbon as an electrode material has some advantages, such as abundance in nature, low cost, chemical and thermal stability, non-toxicity and controlled pore structure, high surface area and high conductivity. However, to be used in double-layer supercapacitors, carbon must meet three important properties: i) high specific surface area in the order of 1000 m^2/g, ii) intra and inter-particle porous conductivity and iii) high electrolyte ion accessibility to the intra-pore space of the electrode[12]. High surface area carbon includes activated carbon, carbon aerogels, carbon nanotubes, templated porous carbons and carbon nanofibers, all are less abundant and more expensive compared to ordinary activated carbons and graphites. The specific capacitance of carbon supercapacitors have been documented as 75-175 Fg^{-1} for aqueous electrolytes and 40-100 Fg^{-1} for organic electrolytes, though generally the value is comparatively lower in practical cases[12]. To improve the capacitance through the increase of the specific surface area, there has been different attempts to modify the surface structure of carbon such as heat treatment, alkaline treatment, steam or CO_2 activation. These processes can lead to defects on the surface of the carbon resulting in higher specific area. The surface modification of carbon materials with heteroatoms or different functional units can be used to enhance the hydrophilicity/lipophilicity of the surface to have increased wettability and rapid access of electrolyte ions in the micropores, resulting in an effective way of leveraging the capacitance from about 5% to 10%. Oxygen, nitrogen, boron and sulphur are the most common functional units that have been used in carbon frameworks, with nitrogen as the most widely investigated. The effect of these functional units has not always been advantageous, especially for the oxygen containing acidic groups as depending on the concentration of functional units and operating voltage, electrolytes may show increased decomposition. For example, nitrogen doped mesoporous carbon was synthesized by Yang *et al*[13]*.* The surface area of the mesoporous carbon was calculated as 663 m^2g^{-1} and the capacitance value was 190 Fg^{-1} [13]. Porter *et al*[14] evaluated the performance of a mixture of activated carbon and 15% carbon nanotubes in organic electrolytes and found specific capacitance values of 90 Fg^{-1} [14].

In summary, carbon materials having high specific surface area and porous structure are good choice as supercapacitor electrode materials in terms of high cycle life and specific power. But the internal resistance can be high because of the carbon contact resistance leading to reduced performances. Research is currently focused on acquiring higher specific surface area, compatible pore distribution and appropriate sizes of carbon for supercapacitor electrodes.

1.4.2 Conducting polymers

Conducting polymers are pseudocapacitive materials. Reversible redox reactions occur in the bulk of

the electrode. During oxidation, ions are transferred to the polymer backbone and during reduction they are released to the electrolyte again. No structural changes occur on the electrode materials, fully reversible process during the charge and discharge mechanism. Advantages of conducting polymers are high storage capacity, large voltage window and can be easily surface modified for better redox potential[12]. The most common conducting polymers for supercapacitor applications are polyaniline, polypyrrol, polythiophene and their derivatives.

Polymers can be doped by oxidation-reduction of the repeating units. By oxidation, polymers become positively charged and denoted as 'p-doped'. By reduction, negatively charged polymers appear and are named as 'n-doped'. Polyaniline and polypyrrols are generally p-doped as the reduction potential is very low. Polythiophene can be both p-doped and n-doped[12]. The specific capacitance for doped conducting polymer electrodes with very high surface area can reach up to 400-500 Fg^{-1} of active materials[5].

The operating potential window for conducting polymers must be carefully controlled. At extended applied voltage, outside the operative range, the polymers can be degraded. At lower potentials, they can become un-doped. Another disadvantage is instability of the structure caused by swelling and shrinking during the intercalation process. These instabilities cause mechanical degradation during the operation of the supercapacitor and may show significant degradation after less than a thousand cycles. This low cycling stability is a challenge for the use of the polymer-based supercapacitors. Different ways to improve polymer characteristics have been investigated.

Modification of the structures to the nanoscale is one of the ways to overcome the limitations of mechanical instability and low cycle life. Conducting polymer based nanorods, nanotubes, nanowires and nanofibers reduce these problems by providing shorter diffusion length[12]. Fabrication of composite polymer materials can ensure higher cycle stability by improving the polymer structure and by reducing mechanical stress. Carbon nanotubes (CNTs) play an important role as a composite material with the polymers giving higher nanostructured porous morphology, high stability, high ionic conductivity, high charge transport and reduction of cycle degradation[12]. For example, a study revealed the maximum specific capacitance of 421.5 Fg^{-1} which was obtained for hybrid polyaniline electrodes with 20 wt% CNF loading as a composite substrate at a current density of 1 Ag^{-1} [15]. Hybrid supercapacitors can be used to maintain good performance with high cycling stability using p-doped polymers as the positive electrode and carbon as the negative electrode. For example Polythiophene as the positive electrode and activated carbon as negative electrode in a hybrid supercapacitor gives higher cycle stability up to 10000 cycles[12].

Though several modifications have been done to have better performance from conducting polymers regarding different parameters with different compounds, there are challenges that still need to be overcome, and more work shall be done in this regard.

1.4.3 Transition metal oxides/hydroxides

Metal oxides provide higher energy density compared to carbon materials and higher mechanical

stability compared to polymer-based materials. The oxides should have high conductivity and should allow protons intercalating in the metal structure during reduction. Researchers have investigated different metal oxides including ruthenium oxide, manganese oxide, cobalt oxide, nickel oxide and vanadium oxide[12].

RuO_2 is the most extensively studied metal oxide in this area because of its high conductivity, long cycle life, tremendous specific capacitance, wide potential window, high reversible redox reactions, multiple accessible oxide states within 1.2 V[10]. RuO_2 has pseudo-capacitive electrochemical response. To have higher specific capacitance, it is very important to have high specific surface area. So different attempts have been taken to increase the surface area of RuO_2 such as producing nanosized oxides or depositing thin films on rough surfaces. Xia *et al*[16] used nanocrystalline RuO_2 to build a symmetric supercapacitor with high operating voltage of 1.6 V. The supercapacitor exhibited an energy density of 18.77 Wh kg^{-1} at a power density of 500 W kg^{-1} [16]. However, ruthenium is very toxic as well as highly expensive metal. Due to its high capacitance, use of small amount of RuO_2 with other metal oxides as composite can be another way of modification. Other metal oxides are also being investigated to have high capacitance values.

MnO_x is another metal oxide which has advantages of low cost, low toxicity, environmental sustainability with higher theoretical specific capacitance of around 1000 Fg^{-1}[12]. Thus, it has been investigated as an alternative electrode option for supercapacitors. The morphology, crystallinity and the oxide or hydroxide state largely influence the pseudocapacitive performance of Mn oxides as electrode material[5]. Smaller surface area, low ionic and electronic conductivity, dissolution of the structure in the electrolyte are some challenges that hinders the performance. Nanostructure formation as a form of surface modification, different crystal structure and composite formation with other metallic structures are ways to improve the performances. For example, single-crystal α-MnO_2 nanotubes prepared by hydrothermal method exhibited 213 Fg^{-1} at a scan rate of 10 mVs^{-1} [17] .

NiO is another alternative as an electrode material for supercapacitors. The advantages of NiO are its high specific capacitance, environment friendliness and reasonable price. NiO is mainly used in alkaline electrolytes. The main challenges regarding the use of NiO are poor cycle performance & poor electrical conductivity[12]. Nanostructure of nickel oxide/hydroxide-based material produced by different methods can enhance the electrochemical performance of the material[18]. Researches regarding cycling stability and good conductivity of the Ni oxide-based materials are being investigated. Ni/metal oxides composite can be a solution to have high conductivity and the asymmetric metal structure may lead to large number of active sites that provide higher surface reaction opportunity. For example, nanostructured Co-Ni/Co-Ni oxide with a cauliflower like shape showed low resistance, with high specific capacitance of 331 Fg^{-1} and high cycling stability[19].

Iron oxides of different forms such as Fe_2O_3, Fe_3O_4, Fe_xO_y, FeOOH have been investigated through numerous researches[20] for supercapacitor application. Iron oxides are cheaper as well as have very low environmental impact. But two major challenges regarding the use of iron oxides as electrode materials are poor conductivity and capacitance decay[20]. All the forms of iron oxides have been used either in

pure form or composite of iron oxides with graphene, carbon or other materials. Zhu *et al*[21] doped Mn_2O_4 with Fe_3O_4 and the composite retained 76% after 5000 cycles at 5 Ag^{-1} with a specific capacity of 448 Fg^{-1} at 5 mVs^{-1} [21]. Another study showed the FeO_x intertwined with carbon nanotubes formed by spray deposition, presented capacitance of 176 Fg^{-1} at a scan rate of 2 mVs^{-1} [22].

Among the many transition metal oxides, cobalt oxide is of special interest given its high theoretical capacitance, high reversibility, large surface area as well as high conductivity[12]. Cobalt oxide Co_3O_4 possess pseudocapacitive behaviour. For example, Co_3O_4 nanowires grown on carbon nanofiber paper collectors presented as brush like morphology exhibits specific capacitance of 1525 Fg^{-1} while on graphite structure the shape takes flower like morphology with a lower value of 1199 Fg^{-1} [23]. Feng *et al*[24] demonstrated large scale preparation of sub-3 nano atomic layers Co_3O_4 nanofilms with substrate free and non-surfactant hydrothermal process. The electrochemical tests revealed nanofilms exhibiting as high specific capacitance as 1400 Fg^{-1} and a very small capacitance degradation after 1500 cycles[24]. Subramani *et al*[25] have developed nanocomposite of Co_3O_4 and reduced graphene oxide(rGO) by co-precipitation method. The specific capacitance of the nanocomposite has been investigated at 1 Ag^{-1} current density in alkaline media and found to be 784 Fg^{-1}. Asymmetric device fabricated with rGO as anode and Co_3O_4/ rGO as cathode exhibited specific capacitance of 245 Fg^{-1} with high energy and power density of 16.6 Wh kg^{-1} and 3473 Wkg^{-1}, respectively[25]. Gómez *et al*[26] produced electrochemically reduced graphene oxide/cobalt oxide (CoO_x) composite by co-electrodeposition with cyclic voltammetry. The produced composite exhibited specific capacitance of 608 Fg^{-1} at a current density of 1 Ag^{-1} and increased reversibility when compared to single CoO_x[26]. Another study by Gómez *et al*[27] revealed reduced graphene oxide/cobalt oxide electrode composites prepared by one step pulsed electrodeposition as a promising electrode material for application in redox supercapacitors, attaining specific capacitance of about 430 Fg^{-1} at 1 Ag^{-1} and presenting long-term cycling ability[27].

Other metal oxides such as V_2O_5, SnO_2 have been investigated to have preferable electrochemical properties to use as electrodes in supercapacitors. All metal oxides and hydroxides present their own merits and limitations, which have led researchers searching different options.

1.5 Nanofoams for supercapacitors

The required demand of higher energy density and longer life cycle have inspired the use of nanostructures for supercapacitor electrodes. Different nanostructures have been documented in the literature classified as zero dimensional, one dimensional, two dimensional and three-dimensional nanomaterials[28]. Zero dimensional nanostructures include uniform particle arrays (quantum dots), nanoparticles, heterogenous particle arrays, hollow spheres and solid spheres. One dimensional nanomaterial comprises nanowires, nanoribbons, nanobelts, nanorods, nanotubes and hierarchical nanostructures. The two-dimensional nanomaterials group consist of branched structures, nanoprisms, nanoplates, nanosheets, nanodiscs and nanowalls. However, 3D architectures have been of special

interest because of their low density and larger specific surface area containing micro, meso or macro-interconnected pores that involve rapid mass transfers and higher molecular transportability[28] . Three dimensional nanostructures are comprised of nanocoils, nanocones, nanoballs, metal nanofoams, nanopillars and nanoflowers[29]. Among these nanostructures, many of them have been used in electrochemical energy storage and specially in supercapacitors because of their high surface area such as carbon-carbon nanotubes, activated carbons, hybrid metal foams, carbon flowers, reduced graphene oxides etc.

3D metallic foams have been of interest in the recent past because of their low cost, easy fabrication, high porosity, high thermal and electrical conductivities and light weight with high surface area[30]. Metal foams have been important in heat exchangers, filters and energy/sound absorbers. The use of metal foams in Li-ion batteries, supercapacitors, fuel cells and sensors have received recent attention. Several methods such as sintering/annealing of metals with gas, filler or blowing agents, deposition of foreign material on metal surface and dealloying by chemical dissolution or burning[31], etching ligaments of the metal surface[30], dynamic hydrogen bubble template[32] etc are used for metal foam fabrication.

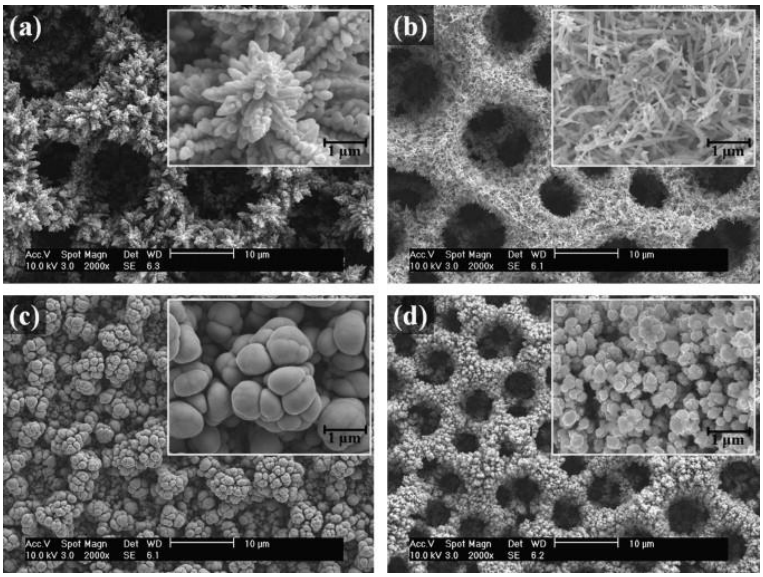

Figure 1.5 Copper nanofoam structures deposited at different conditions [33]

Dynamic Hydrogen bubble template (DHBT) method is a clean and efficient one step synthesis process where hydrogen bubbles (generated by electrodeposition at high overpotentials[34]) act as a dynamic template, around which the metal deposition occurs. Hydrogen evolution due to high cathodic overpotential modifies the metal deposition providing honeycomb like morphology. The H_2 evolution is vigorous enough that it can change the hydrodynamic structure of the electrode surface providing microporous cauliflower or dendrite-like nanostructures. The morphology and porosity of the foam can be controlled by tuning the electrodeposition parameters and are independent of the potentiostatic and galvanostatic regime of electrolysis[34].

The DHBT method involves three steps for H_2 evolution: nucleation, growth and detachment. During the deposition, on the active sites of the substrate, H_2 nucleation occurs simultaneously with the metal nuclei. The growth of bubble size ensures decreased contact angle with the electrode until detachment.

During detachment, the bubbles leave regular holes in the deposited metal morphology. Some new and fresh bubbles can coalesce with the bubbles already formed at the initial stage of the electrodeposition. Irregular holes are formed due to the agglomerate metal grains between the bubbles. Some small bubbles that cannot coalesce, detach leaving channels in the interior of the deposits. For longer time of electrodeposition, coalesced bubbles form coalesced holes [34].

The reactions occurring in the electrodeposition process are shown in equation (1.3) and (1.4)[32].

$$2H^{+}_{(aq)} + 2e^{-} \rightarrow H_{2(g)} \quad (1.2)$$

$$M^{n+}_{(aq)} + ne^{-} \rightarrow M_{(s)} \quad (1.3)$$

The number, size and orientation of the holes depend on several factors like regimes of electrolysis, concentration of depositing ions, concentration of supporting electrolyte, preparation of working electrode and time of electrolysis[34]. The increase of overpotential or current density increases the number of holes formed by the detachment of H_2 bubbles. Higher concentration of the metal ions lessens the average current efficiencies for H_2 evolution reaction while higher concentration of the supporting electrolytes (H_2SO_4, NH_4Cl, HNO_3 etc) increases the average current efficiencies resulting in increased H_2 bubble formation. H_2 nucleation occurs on the active sites of the working electrode which can increase because of surface irregularities, defects and edges[32]. The size of the holes accelerates with the deposition time due to the increase of hydrogen bubbles and coalescence among them. Less electrolysis time can cause the lowering of current density distribution which results the hydrogen bubbles being captive in the foams leaving porous structure[34]. Different monometallic and bimetallic foams have been documented to be fabricated by DHBT method such as Pt, Cu, Ni, Co, CuNi, NiCo, NiCu, NiSn, PtPd, CuPt etc[32].

These metallic foams have been investigated for use in Li batteries, sensing applications, electrocatalysis, capacitors etc. For use in capacitors, metallic foams need post treatment to convert it to oxides and/or hydroxides possessing pseudocapacitive properties. A recent study showed the effect of electrodeposited manganese oxide on bimetallic Ni-Co nanofoam as a composite electrode for supercapacitor application. The 3-D nanofoam structure was achieved by the DHBT method to get high surface area and tailored porosity. Enrichment of nickel foam with cobalt ensured lower density structure compared to nickel foam alone. This composite electrode exhibits high charge discharge rate capabilities of 91% capacitance retention at 20 Ag^{-1} with enhanced electrochemical performance having capacitance of 194 Fg^{-1} at 0.5 Ag^{-1} current density[35].

The 3-D nanostructure of cobalt can ensure high surface area with high porosity which is an important requirement to be used as electrode materials. The present study explores the possibility of producing Co nanfoams via the DHBT electrodeposition method, tailoring their porosity and surface area, modification of the nanofoams to cobalt oxides and evaluate their energy storage performances.

1.6 Properties of cobalt & formation of cobalt oxides

Cobalt (Co) is a transition metal appearing on the Group 9 of periodic tables of elements between iron and nickel. Cobalt is mainly found in the earth crust and has been used as a colouring agent mainly for glass and pottery at least for 2600 years in Persia and Egypt[36]. The properties of Cobalt are presented on Table 1.3.

Table 1.3 Physical properties of cobalt [37]

Symbol	Co
Atomic number	27
Atomic weight	58.933
Electron configuration	$[Ar]3d^74s^2$
Valence	+2 and +3, other also known 0, +1, +4 and +5
Isotopes	Co-59 (99.8%) and Co-57 (0.2%)

The usage of cobalt has become more in technical based sectors such as medical diagnostics, pharmaceuticals, fermentation processes and is not replaceable with any alternative. The demand in chemical sector has significantly increased recently because of its application in rechargeable batteries. European Union and USA have listed Cobalt respectively as 'critical' and 'strategically important' in 2011 because of its industrial and technological importance[36].

Cobalt is a magnetic metal and have three different crystal structures: hexagonal closed packed (hcp) (α-phase), face-centred cubic (fcc) (β-phase) and primitive cubic phase (ε-phase). The α-phase predominates at temperatures up to 417^0C while β-phase is more common above this temperature. Metastable ε-phase can only be synthesized through solution-phase processes and can be converted to α or β-phases by annealing at suitable temperatures[37,38].

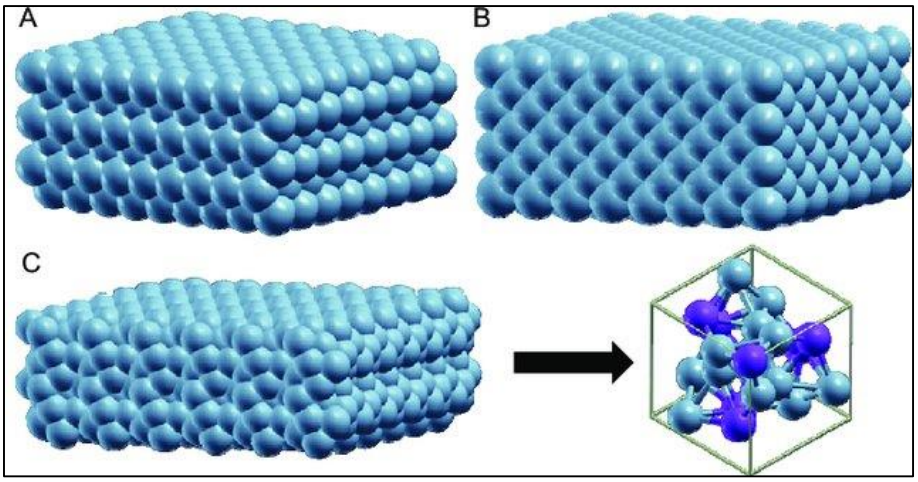

Figure 1.6 Structures of cobalt phases A) α-phase, B) β-phase and C) ε-phase including a detail of the different cobalt positions [38]

Cobalt oxides are very popular for CO sensors, rechargeable batteries or as catalyst in CO reduction. Five forms of cobalt oxides have been reported in literature: CoO_2, Co_2O_3, CoO(OH), Co_3O_4 and CoO. Among all of them, CoO and Co_3O_4 are most common and thermodynamically stable.

CoO is an antiferromagnetic material and has a face centred cubic structure. The valence state is +2 and density is 6.44 g cm^{-3} [37]. CoO has been extensively studied because of its catalytic activity and application in gas sensors. Studies have been carried out for enhanced electrochemical properties of CoO for supercapacitor applications[39]. Co_3O_4 is another antiferromagnetic material with a spinel structure. The structure contains Co^{2+} ions octahedrally coordinated and Co_2^{3+} as tetrahedrally coordinated with oxygen ions. Valence state is +8/3 and density is 6.11 g cm^{-3} [37]. Wang *et al*[40] showed that CoO, which is a p type oxide, can be oxidized to Co_3O_4(n-type oxide) at 500^0C which eventually decomposes back to CoO. Co_3O_4 is dominant at $500^0C<T<1000^0$C and CoO is dominant at $T>1000^0$C upon oxidation[40]. Tompkins *et al*[41] studied the oxidation behaviour of cobalt from room temperature to 467^0C. The study showed at room temperature $Co(OH)_2$ forms, from 100^0 to 225^0C, the CoO films are formed and at higher temperatures than 425^0C, a mixture of Co_3O_4 and CoO or pure Co_3O_4 appears. According to Tang *et al*[42], the oxidation of CoO to Co_3O_4 occurs at 250^0C and decomposes back to CoO at about 900^0C.

The stability of different phases of Co-H_2O system with regard to solution pH and voltage potential is explained by the Pourbaix diagram for Cobalt–H_2O system in Figure 1.7. Co metal oxidizes to Co^{2+} form when the voltage is positive, and pH is less than 8. $Co(OH)_2$ is the passivation layer and is stable in the pH range from 9 to 13. $Co(OH)_2$ oxidizes to $Co(OH)_3$ form when the potential increases than 1V.

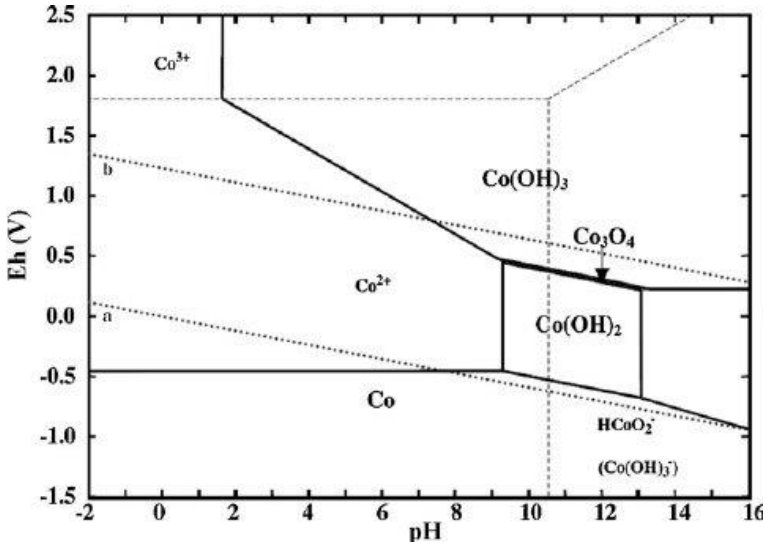

Figure 1.7 Pourbaix diagram for the Cobalt – H_2O system[43]

The electrochemical oxidation of Cobalt with potassium hydroxide electrolyte was documented by Behl *et al*[44] where, anodic oxidation of cobalt occurred only in the solid phase and produced $Co(OH)_2$ film at first. $Co(OH)_2$ can be potentiostatically oxidized to Co_3O_4 , which can further by oxidized to CoOOH by the application of higher potentials. $Co(OH)_2$ was dissolved at all concentrations of KOH while Co_3O_4 and CoOOH have negligible solubility. The passivation layer near the cobalt metal surface was mainly associated to the formation of a CoO film[44].

This study does not relate immediately with the Pourbaix diagram. In fact $Co(OH)_2$ should be stable in pH form 9 – 13 (not dissolving) and the passive layer in the diagram is $Co(OH)_2$ (not CoO). Also, CoOOH does not appear in the Pourbaix diagram.

In summary, the use of cobalt has become very popular for technological purposes in past years. Co oxides has also been investigated for use in energy storage because of its excellent conductivity, high reversibility and high theoretical capacity. The aim of this research work is to evaluate the electrochemical properties of Co nanofoam produced by DHBT electrodeposition method. Physico-chemical properties of the nanofoams will be assessed with different characterization methods. Thermal, chemical and electrochemical treatment of the Co foam will be carried out to convert the metallic Co structure to cobalt oxide and hydroxide. Physico-chemical and electrochemical properties of the treated nanofoams will be evaluated and the comparison of the response of the untreated and treated samples will be presented. Electrochemical cell assembled with the Co nanofoam and the best treated Co nanofoams will be evaluated with electrochemical measurements.

.

Chapter 2

Experimental Procedure

This Chapter includes all the experimental steps followed during this research activity. Preparation procedure of cobalt nanofoam by DHBT electrodeposition method and treatment of the nanofoams with different oxidation techniques have been documented. All the experimental conditions, parameters, materials and the instruments used throughout the experiment are specified. Physico-chemical and electrochemical characterization procedure along with all the parameters and conditions are also documented in this chapter.

2.1 Materials and solution preparation

2.1.1 Preparation of the Co nanofoam

AISI 304 stainless steel (Fe/Cr18/Ni10) plate from *GoodFellow*® was used as current collector for the metal foam deposition. The substrates were 2.5cm × 2.5cm with an area of about ~6.25 cm^2.The substrates were polished at first to have a uniform, smooth and clean surface with SiC abrasive paper from *BUEHLER*® of P360, P600 and P1000 grit. After polishing, the substrates were rinsed respectively with distilled water and ethanol. Then the substrates were dried with compressed air. Finally, the weight of each substrate was measured with *Sarotius* MC5-0CE micro-balance with an accuracy of 0.01mg.

An aqueous solution of 0.1M $CoCl_2 \cdot 6H_2O$ *(Carl ROTH)* and 2M NH_4Cl (*Carl ROTH*) was prepared for foam deposition. The foam deposition was carried out with a two-electrode electrochemical cell connected with *Sorensen LH 110* DC power supply. AISI 304 stainless steel was the working electrode and Pt was used as a counter electrode of the electrochemical cell. The cylindrical cell was about 7 cm of height and about 4 cm of diameter. A lateral hole with a diameter of 0.9 cm where the working electrode attached contains an O-ring to prevent the leakage of the electrolyte. A current density of -2.83 A/cm^2 was applied for 30 seconds. After the foam deposition, the samples were rinsed respectively with distilled water and ethanol followed by drying with compressed air. Finally, the samples were dried at room temperature and the weight of the active material was carefully meassured with the micro-balance.

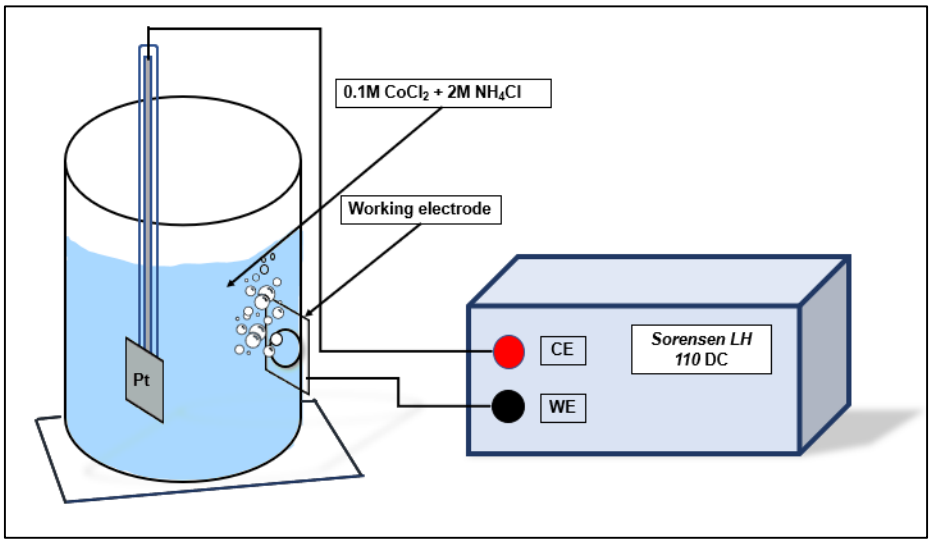

Figure 2.1 Electrochemical setup for foam fabrication

2.1.2 Thermal treatment

Prepared foams were thermally treated for oxidization at different temperatures for 3 hours at 100^0C, 150^0C, 200^0C, 250^0C, 300^0C in a *Memmert* oven and at 400^0C in a muffle furnace (*SNOL*). After the thermal oxidation, the samples were cooled down at room temperature and the weight of the oxidized

active material was measured. After treatment, samples were measured in 1M KOH.

2.1.3 Chemical treatment

For chemical oxidation, hydrogen peroxide was used as an oxidizing agent in different concentrations for different times. 35% H_2O_2 (*MERCK*) was diluted to desired concentrations of 5%, 10% and 20%, and samples were immerged in 10mL of each solution for 1h, 4h, 8h, 16h, and 24h. After the treatment, samples were air dried and kept at room temperature for at least 24 hours. The weight of oxidized active material was measured with micro-balance before measuring in 1M KOH.

2.1.4 Electrochemical polarization

Prepared nanofoams were electrochemically polarized with a three-electrode electrochemical cell (Figure 2.2) connected to *Gamry Reference 600* potentiostat. The working electrode of the sample was the Co foam deposited on stainless steel. A spiral Pt electrode was used as the counter electrode and saturated calomel electrode (SCE) acted as the reference electrode. The samples were polarized at two different potentials of 0.4V and 1.1V in 1M KOH.

2.2 Electrochemical measurements

The electrochemical measurements were carried out with a three-electrode electrochemical cell explained in section 2.1.4. 1M KOH (*Sigma Aldrich*) was the electrolyte used for the electrochemical measurements.

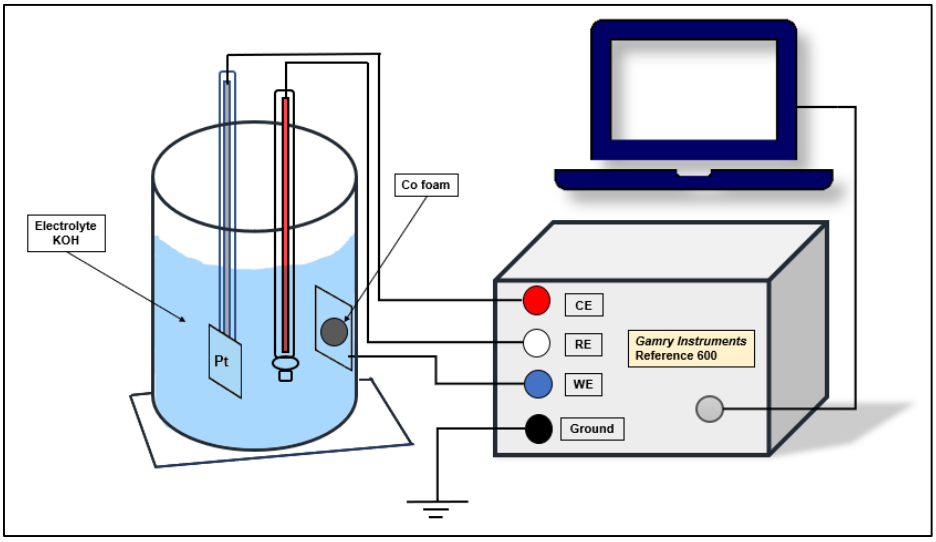

Figure 2.2 Three electrodes electrochemical cell

Cyclic voltammetry of the untreated nanofoams were carried out at a potential range from -0.6 V to 0.4 V at different scan rates, ranging from 20 mVs^{-1} to 200 mVs^{-1}. Prior to the measurements, samples

required an activation process of 20 cycles in the same potential range for stabilization. The potential windows of cyclic voltammetry for chemically oxidized nanofoams and Co nanofoams treated at higher temperatures were generally ranged from -0.6 V to 0.6 V. Nanofoams treated at lower temperatures than 250^0C, were measured at the same condition of the untreated nanofoams.

The potential window for galvanostatic charge discharge was -0.6 V to 0.4 V for untreated nanofoam and nanofoams treated at lower temperatures than 250^0C, while for higher temperature and chemically treated nanofoams the range was -0.6 V to 0.6 V. Different current densities were applied, ranging between 1 Ag^{-1} and 10 Ag^{-1}. The coulombic efficiency of the Co nanofoam was measured using the equation (2.1)[7]

$$\eta = \frac{t_D}{t_C} \times 100\% \qquad (2.1)$$

where, η is the coulombic efficiency, t_D is the discharge time and t_C is the charging time.

The specific capacitance was evaluated using the galvanostatic charge discharge data with the following equation[7].

$$C = \frac{I\,\Delta t}{m\Delta V} \qquad (2.2)$$

where, I denotes current applied to the sample, m is the mass of the active material, Δt is the time and ΔV denotes the total voltage applied.

Cycling stability of the material was tested with 2000 galvanostatic charge discharge cycles in the potential range from -0.6 V to 0.4 V for Co nanofoam and from -0.6 V to 0.6 V for the chemically treated Co nanofoam. Capacitance retention after n number of cycles were calculated by

$$Capacitance\ retention\ (\%) = \frac{C_n}{C_1} \times 100 \qquad (2.3)$$

where, C_n is the specific capacitance after n^{th} cycle and C_1 is specific capacitance after 1^{st} cycle.

Electrochemical Impedance Spectroscopy (EIS) of Co nanofoams was measured at two different potentials of -0.35 V and 0.35 V corresponding, respectively, to discharged and charged state. A conditioning pre-step was carried out for 500 sec and then EIS was measured by applying a sinusoidal perturbation with 10 mV (rms) amplitude in the frequency range of 10^{-2} Hz to 10^5 Hz. The capacitive behaviour of the Co nanofoam was measured by calculating capacitance dependent on frequency, defined as[45]

$$C(\omega) = C'(\omega) + C''(\omega) \qquad (2.4)$$

where,

$$C'(\omega) = \frac{-Z''(\omega)}{\omega|Z(\omega)|^2} \qquad (2.5)$$

$$C''(\omega) = \frac{Z'(\omega)}{\omega|Z(\omega)|^2} \qquad (2.6)$$

and

$$Z(\omega) = Z'(\omega) + Z''(\omega) \qquad (2.7)$$

Where $C'(\omega)$ and $C''(\omega)$ indicate the real and imaginary part of the complex capacitance respectively and $Z'(\omega)$ and $Z''(\omega)$ are the real and imaginary impedance dependent on the frequency, respectively.

Self-discharge rate of the Co nanofoam was measured after charging for 1800s and discharge was carried out for 3600s.

2.2.1 Effect of electrolyte concentration

Effect of the electrolyte concentration on the electrochemical measurements was carried out with different concentration of KOH between 0.1M to 4M. Cyclic voltammetry for different scan rates and galvanostatic charge discharge for different current densities were measured.

2.3 Electrochemical cell set up

To assess the potential application of the nanofoams in cells, different symmetric and asymmetric cells were fabricated. Two different symmetric electrochemical cells were assembled with Co nanofoams and chemically treated Co nanofoams (5% H_2O_2 24h). For asymmetric cells, commercial carbon was used as the negative electrode. One asymmetric cell was assembled with Co nanofoam while another with chemically treated Co nanofoam (5% H_2O_2 24h) as the positive electrodes. For asymmetric cell, the mass balance between the two electrodes was maintained by charge balance of the two electrodes $q_+=q_-$ calculated from the following equations[25].

$$q_+ = C_+ \times \Delta V_+ \times m_+ \quad (2.8)$$

$$q_- = C_- \times \Delta V_- \times m_- \quad (2.9)$$

$$C_+ \times \Delta V_+ \times m_+ = C_- \times \Delta V_- \times m_- \quad (2.10)$$

$$\frac{m_+}{m_-} = \frac{C_- \times \Delta V_-}{C_+ \times \Delta V_+} \quad (2.11)$$

where, m_+ and m_- are mass of Co nanofoam and carbon active material respectively. C_+ and C_- are capacitance and $\Delta V_+$and ΔV_- are potential range for positive and negative electrode, respectively. The electrochemical properties of carbon electrode and the symmetric and asymmetric cells were measured in 1 M KOH. Before setting up the cell, both untreated and treated Co nanofoams were stabilized with 20 cycles of cyclic voltammetry in 1 M KOH to have stable response. Cyclic voltammetry, galvanostatic charge discharge and cycling stability measurements of the cells were carried out.

Specific energy and specific power of asymmetric cell of chemically treated Co nanofoam (5% H_2O_2-24h)-carbon was calculated with the following equations[7]:

$$E = \frac{1}{2} C \Delta V^2 \quad (2.12)$$

$$P = \frac{E}{t} \quad (2.13)$$

where, C is specific capacitance (Fg^{-1}), ΔV is potential window (V), t is discharge time (s), E is specific energy ($Wh\ kg^{-1}$) and P is specific power ($kW\ kg^{-1}$)

2.4 Material characterization

Surface morphology and chemical composition of the samples were measured by scanning electron microscopy (SEM) direct imaging, energy dispersive X-ray spectroscopy (EDS) and X-ray diffraction spectroscopy (XRD). SEM direct imaging was carried out to obtain high resolution images of prepared samples with JEOL 7001-F SEM instrument operated at accelerating voltage of 15 keV. The Energy dispersive X-ray spectroscopy (EDS) was conducted to determine the elemental composition of the sample by measuring energy and intensity distribution of the X-ray signal generated by a focused electron beam interaction with the sample. The EDS detector was coupled with the SEM instrument. X-ray diffraction spectroscopy (XRD) was obtained using the Bruker AXS D8 Advance instrument with Cu Kα radiation (1.5418 Å).

Chapter 3

Results and Discussion

3.1 Cobalt nanofoam

3.1.1 Physico-chemical characterization

Scanning electron microscopy (SEM), X-ray diffraction spectroscopy (XRD) and Energy dispersive X-ray spectroscopy (EDS) were used to evaluate the physico-chemical properties of the Co nanofoam.

Figure 3.1 includes the SEM images of the produced Co nanofoam. The images show the morphological features at two different magnifications. It is clearly seen from the image that the Co foam morphology is a highly porous honeycomb like morphology with regular and irregular holes. From the high magnification image, the cauliflower like agglomerates are more visible. Average diameter of the hole is around 15 μm to 18 μm. Some irregular channels connecting the holes among themselves can be observed in the image that are caused by the coalescence.

XRD analysis was carried out for Co nanofoam as explained in section 2.3. The diffractogram contains two defined peaks at 44.5^0 and 50.7^0 presented in Figure 3.2 corresponding to (111) and (200) face-centred cubic structure of cobalt (ICDD-00-001-1259).

Elemental composition of the deposited Co nanofoam was determined with Energy Dispersive X-ray spectroscopy. The EDS indicated the presence of cobalt as expected for the cobalt nanofoam. The atomic percentage of cobalt in the foam was indicated to be about 90% with balance oxygen.

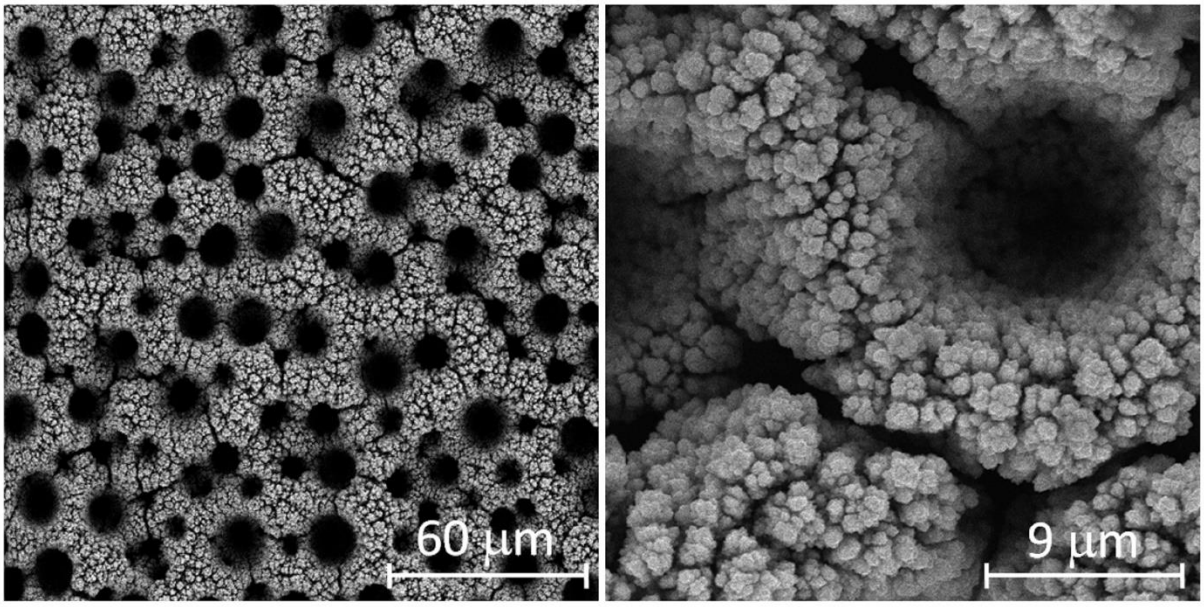

Figure 3.1 SEM images of prepared cobalt nanofoam at (a) 400× & (b) 3000× magnification

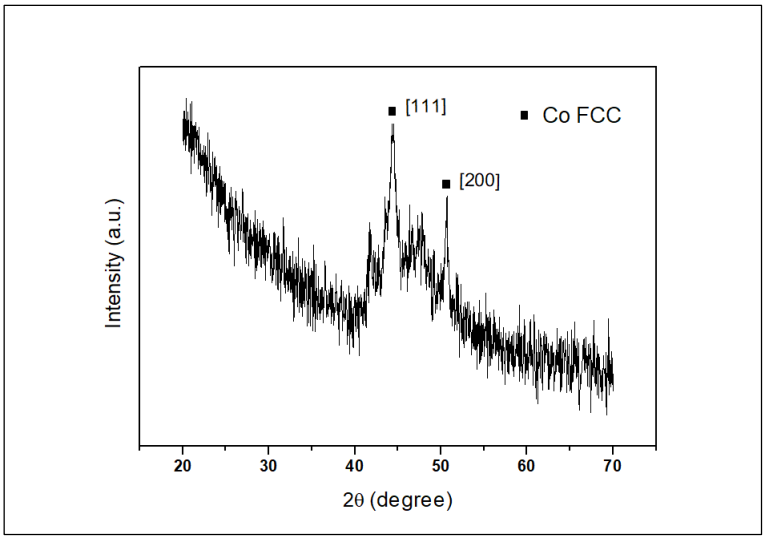

Figure 3.2 XRD spectrum of a pristine Co nanofoam

3.1.2 Electrochemical characterization

Cyclic voltammetry is an important measurement technique for evaluation of electrochemical behaviour of materials for use in electrochemical energy storage systems. The cyclic voltammetry of produced

cobalt nanofoam was performed in the potential range from -0.6 V to 0.4 V in 1 M KOH electrolyte solution at different scan rates ranging from 20 mVs^{-1} to 200 mVs^{-1}. The voltammograms of Co nanofoam in Figure 3.3 clearly exhibit pseudocapacitive response integrated with partial redox intercalation[46]. The increase in current density with scan rate indicates a diffusion-controlled electron transfer process[47]. Also, with the increase of the scan rates, the electrode becomes more resistive and the anodic and cathodic waves become more evident. The anodic and cathodic wave-like responses may be associated with superficial intercalation.

Galvanostatic charge-discharge curves of Co nanofoam, carried out at 1 Ag^{-1} in the potential range from -0.6 V to 0.4 V are shown on Figure 3.4. At initial stage of charging, the electrode is resistive, but after some time the charge and discharge curves both follow almost linear behaviour with some fluctuations indicating the pseudocapacitive response with partial redox intercalation on the Co nanofoam[46]. The Faradaic efficiency calculated from equation 2.1 at 1 Ag^{-1} is found to be 89.9% which indicates small faradaic losses.

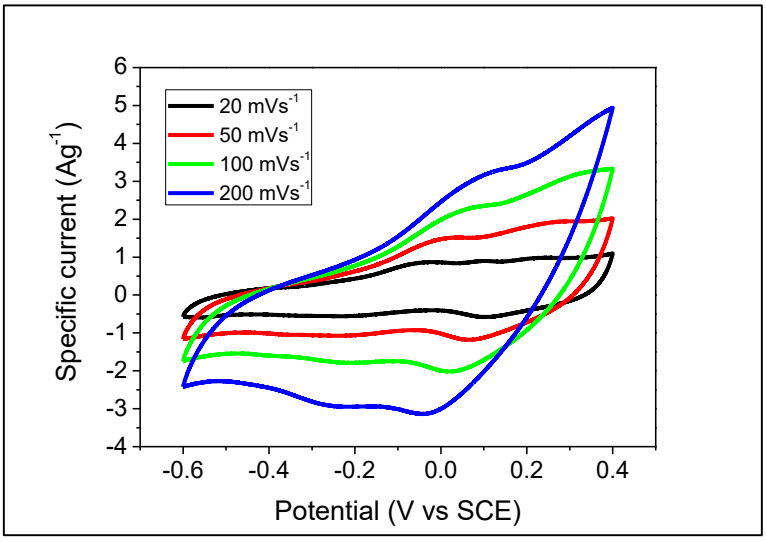

Figure 3.3 Cyclic voltammograms of a Co nanofoam at different scan rates

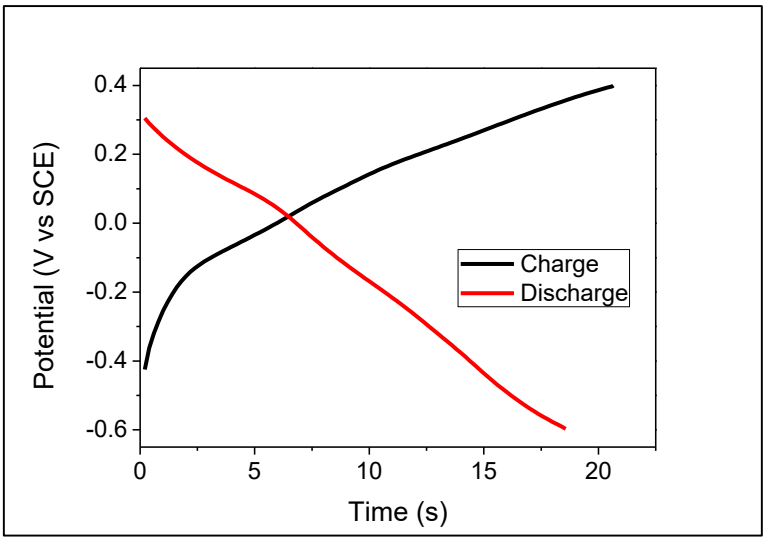

Figure 3.4 Charge - discharge curve of a Co nanofoam at $1Ag^{-1}$

Discharge curves at different specific currents ranging from 1 Ag^{-1} to 6 Ag^{-1} in 1 M KOH, are shown in Figure 3.5. The corresponding specific capacitance for different current densities (equation 2.2) are presented in Table 3.1. The specific capacitance of Co nanofoam is 20.4 Fg^{-1} at 1 Ag^{-1} and exhibits ~36% decrease with a six-fold increase of specific current attaining a capacitance value of 7.3 Fg^{-1} at 6 Ag^{-1}.

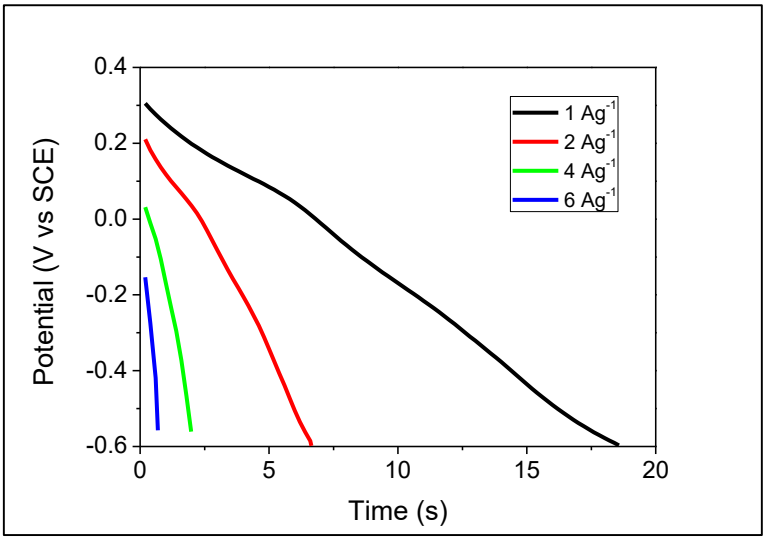

Figure 3.5 Galvanostatic charge-discharge curve of a Co nanofoam at different current densities

Table 3.1 Specific capacitance of a Co nanofoam at different current densities

Specific current Ag^{-1}	**Specific capacitance** Fg^{-1}
1	20.4
2	15.9
4	12
6	7.3

To test the durability of the material, specific capacitance retention was calculated from the discharge curves at 1 Ag^{-1} for 2000 charge discharge cycles. The capacitance stability of the Co nanofoam is depicted in Figure 3.6. The results indicate that the capacitance decreases very fast within the first 200 cycles, after which attains a stable value. This instability of the electrode may because of weak interaction between cobalt nanofoam active material and the substrate stainless steel. Another reason of the instability can be an irreversible reaction.

The Electrochemical Impedance Spectroscopy was carried out for the Co nanofoam at two different potentials, corresponding to the discharged (-0.35 V - Figure 3.7) and charged (0.35 V - Figure 3.8) states. The Bode plots and evolution of real and imaginary capacitance calculated from the experimental data along with the Nyquist plots at discharged and charged states are presented.

The Bode plots indicate a decrease of the resistance and a negative increase of the phase angle in the same frequency range when the material goes from the discharged state to the charged state (Figure 3.7 (a,b) & Figure 3.8 (a,b)). The reason of higher resistance at discharged state can be loss of

electrolyte ions on the electrode surface when the material is discharged.

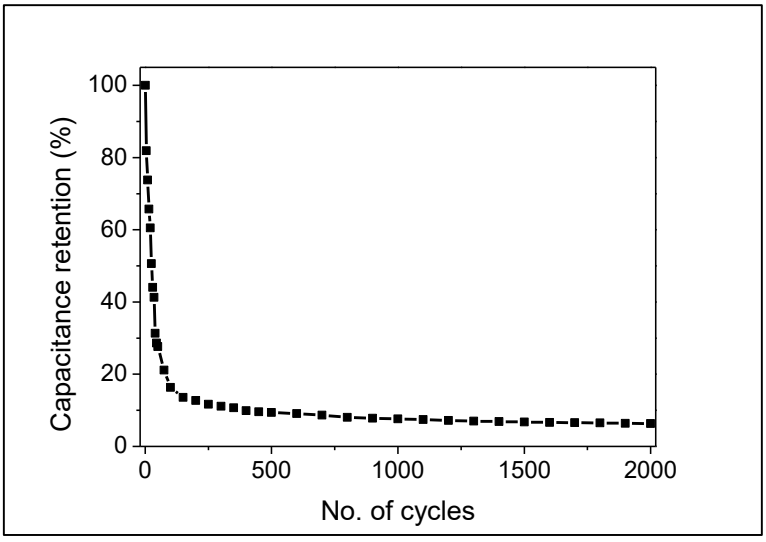

Figure 3.6 Cycling stability of a cobalt nanofoam

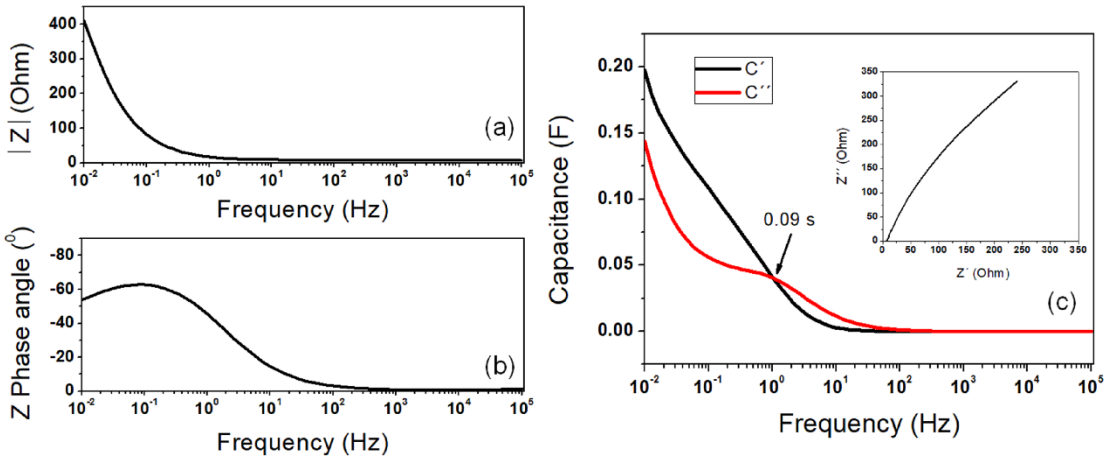

Figure 3.7 Electrochemical Impedance Spectroscopy of a Co nanofoam at discharged state (-0.35V): Bode plots (a, b); evolution of real and imaginary part of capacitance vs Frequency (c) (Nyquist plot in inset);

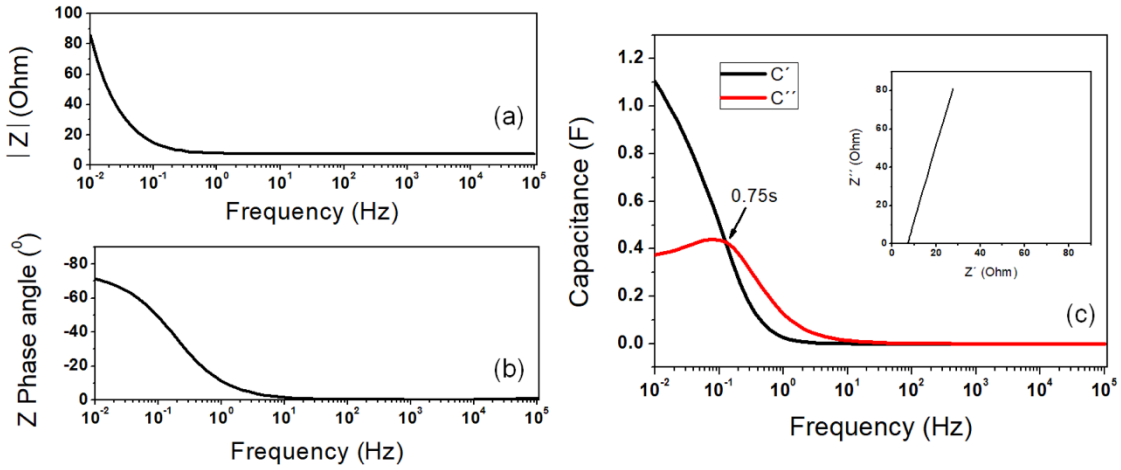

Figure 3.8 Electrochemical Impedance Spectroscopy of a Co nanofoam at charged state (0.35V): Bode plots (a, b); evolution of real and imaginary part of capacitance vs Frequency (c) (Nyquist plot in inset);

The Nyquist plots at discharged state (Figure 3.7(c) inset) and charged state (Figure 3.8(c) inset) show that Co nanofoam exhibits more resistive response during charged state compared to the discharged state. So, the material is more conductive at high potential (0.35V) and more resistive at lower potential (-0.35V).

Real and imaginary part of capacitance depend on frequency respectively, $C'(\omega)$ and $C''(\omega)$ were calculated with the equations from (2.3) to (2.7) from chapter 2. $C'(\omega)$ represents the capacitance of the electrode material and the electrode- electrolyte interaction. For the discharged state at -0.35V (Figure 3.7(c)), at higher frequency, the material shows poor capacitance. As the frequency decreases, at around 100 Hz, the capacitance increases significantly and almost linearly. For the charged state at 0.35V (Figure 3.8(c)), the response at high frequency is similar to the discharged state. The increase in capacitance occurs when the frequency decreases at about 10 Hz and the increase continues exponentially with the lowering of frequency. The reason behind the high capacitive response at low frequency is the good electrode-electrolyte interaction. At lower frequency, electrolyte can reach the porous bulk of the nanofoam and more active materials take part in the storage process. But at higher frequency, the interaction between the electrolyte and the cobalt nanofoam is for very short time and only limited to the surface of the nanofoam.

3.2 Effect of thermal treatment

3.2.1 Physico-chemical characterization

As have been described in chapter 2, produced cobalt nanofoams were treated thermally at different temperatures from 100^0C to 400^0C for 3 hours in air. Physico-chemical characterization of the thermally

treated Co nanofoams at 100^0C and 400^0C was carried out with SEM and XRD measurements. Figure 3.10 presents the SEM images of the nanofoams treated at two different temperatures. The SEM image of the Co nanofoam thermally treated at 100^0C does not show significant differences compared to the untreated Co nanofoam in Figure 3.1. However, when treated at 400^0C, the cauliflower like nanostructures are more agglomerated and a transformation of the morphology is visible compared to the untreated Co nanofoam and treatment at 100^0C. In this case, the morphology may correspond to an oxide layer upon the bare metallic cobalt foam which makes the nano features look more round-shaped aggregates.

XRD diffractograms of the Co nanofoams treated at 100^0C and 400^0C are presented in Figure 3.11. The XRD of nanofoams treated at 100^0C, shows the (111) plane of face-centred cubic cobalt (ICDD-00-001-1259) as seen in Co nanofoam. The (200) plane of Co FCC is not seen, which may have changed to another phase in this case. For treatment at 400^0C, seven peaks at 31.2^0, 36.7^0,38.6^0,44.5^0,55.6^0,59.4^0 and 65.1^0 represents (220), (311), (222), (400), (422), (511) and (440) planes of the face-centred cubic Co_3O_4 (ICDD-00-042-1467), respectively. Three other peaks at 43.5^0, 44.3^0 and 50.5^0 are due to the stainless-steel substrate.

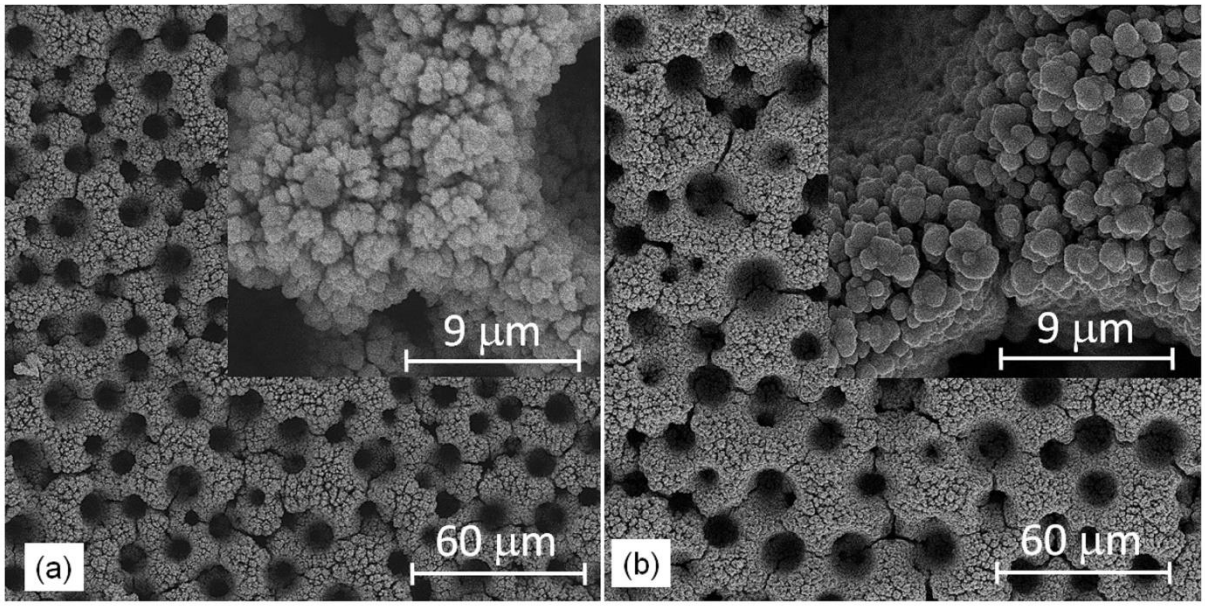

Figure 3.9 SEM images of thermally treated Co nanofoams at (a) 100^0C and (b) 400^0C

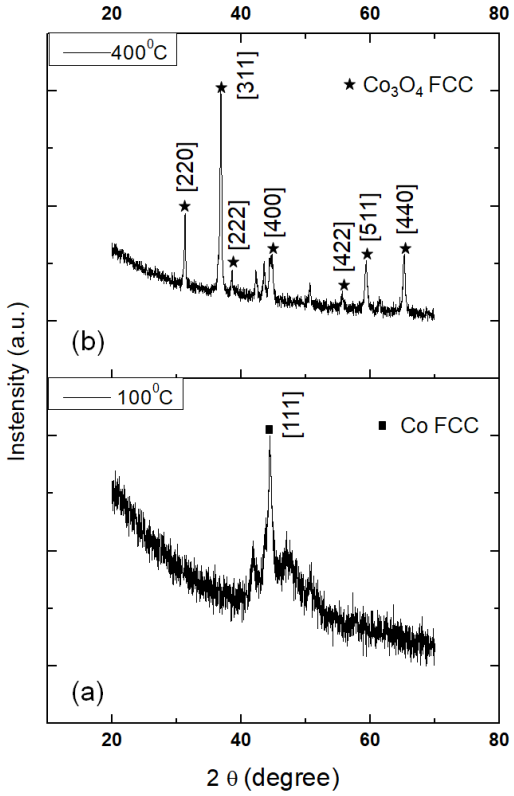

Figure 3.10 XRD spectrum of thermally treated Co nanofoams at (a) 100^{0}C and (b) 400^{0}C

3.2.2 Electrochemical characterization

The electrochemical performance of the treated Co nanofoam was analysed with cyclic voltammetry and galvanostatic charge discharge. The voltammograms of the thermally treated Co nanofoams at different temperatures from 100^{0}C to 400^{0}C for 3 hours are presented in Figure 3.12. The voltammograms obtained for nanofoams heat treated at temperatures lower than 250^{0}C show similar response to the untreated Co nanofoam. The response for 100^{0}C shows that, the surface area under the voltammogram is slightly higher which may be due to the de-hydration of the surface resulting in lower mass which leads to higher specific capacitance. For treatment at temperature higher than 250^{0}C, the voltammogram response is more faradaic dominated with defined peaks compared to the low temperature treatment. At higher temperatures the formation of Co_3O_4 dominates the electrochemical response causing a decrease in conductivity and, as result, a smaller area under the CV curve appears. The oxides are formed at higher temperature due to the presence of oxygen present in the air. The more visible redox peaks for Co nanofoams treated at higher temperatures may be described by the following reactions[25]:

$$Co_3O_4 + OH^- + H_2O \leftrightarrow 3CoOOH + e^-$$

$$CoOOH + OH^- \leftrightarrow CoO_2 + H_2O + e^-$$

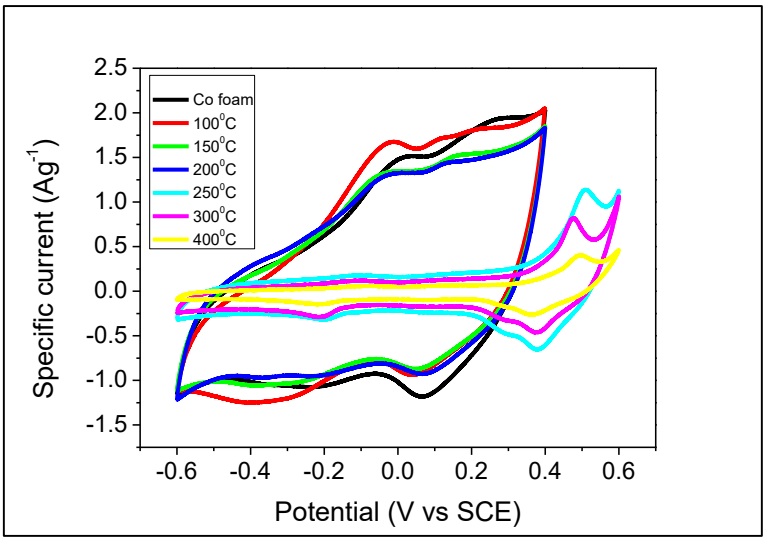

Figure 3.11 Cyclic voltammograms of Co nanofoams after treatment at different temperatures at 50 mVs^{-1}

The discharge curves of the Co nanofoams treated at different temperatures from 100^0C to 400^0C at 1 Ag^{-1} in Figure 3.13 show pseudocapacitive and intercalation feature with partial redox response[46]. At temperatures lower than 250^0C, the discharge time is almost same as for the Co nanofoam. At temperatures higher than 250^0C, more waves appear in the discharge response with significant decrease in discharge time. The response is more faradaic dominated [46]. The specific capacitance for samples treated at 100^0C, 200^0C, 250^0C and 400^0C was calculated at 1 Ag^{-1} and found to be 21 Fg^{-1}, 19 Fg^{-1}, 6.9 Fg^{-1} and 1.4 Fg^{-1}, respectively. So, the increase of temperature above 250^0C leads to significant decrease of the capacitance in accordance with the voltammetry profiles (Figure 3.12).

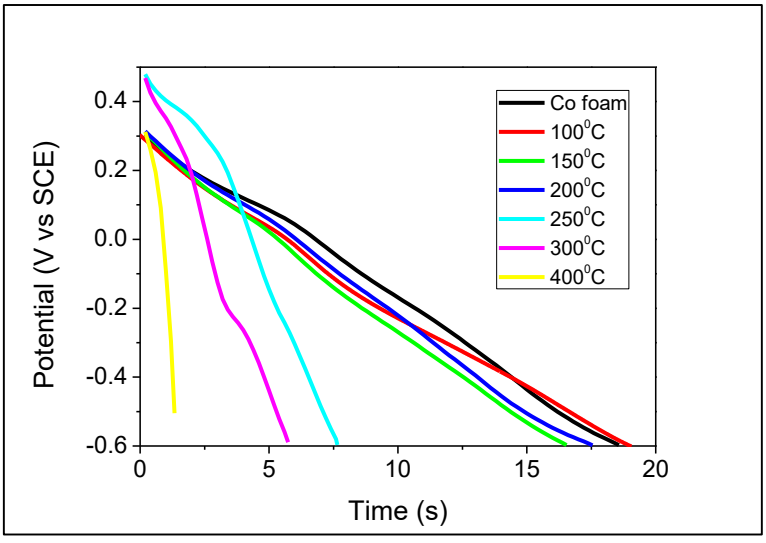

Figure 3.12 Galvanostatic discharge curves of Co nanofoams after treatment at different temperatures at $1Ag^{-1}$

3.2.3 Thermal treatment optimization

Considering the results of thermally treated nanofoams, treatment at 100^{0}C was considered the best result and was repeated for a range of time from 1 hour to 8 hours. The voltammograms are shown in Figure 3.14 that indicate no significant effect of treatment times at 100^{0}C. The discharge curves for nanofoams treated at 100^{0}C for different times are depicted in Figure 3.15 also show similar response and there is no significant change on discharge time for different treatment times.

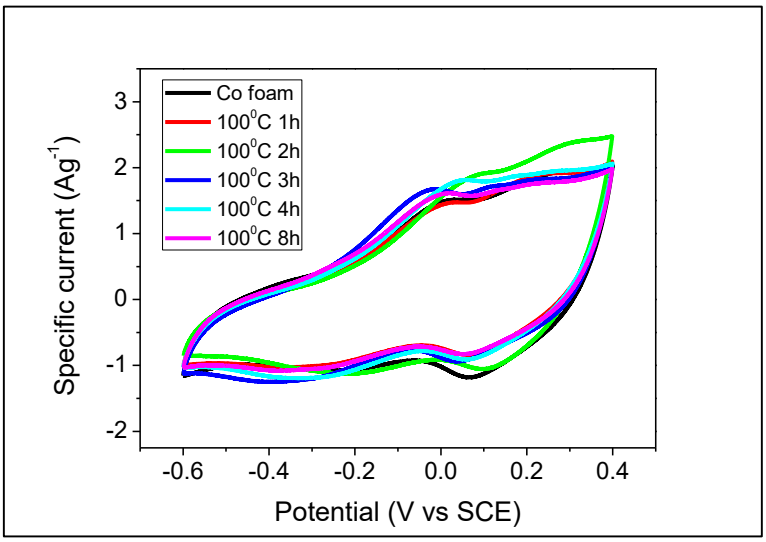

Figure 3.13 Cyclic voltammograms of Co nanofoams treated at 100^{0}C for different times at 50mVs^{-1}

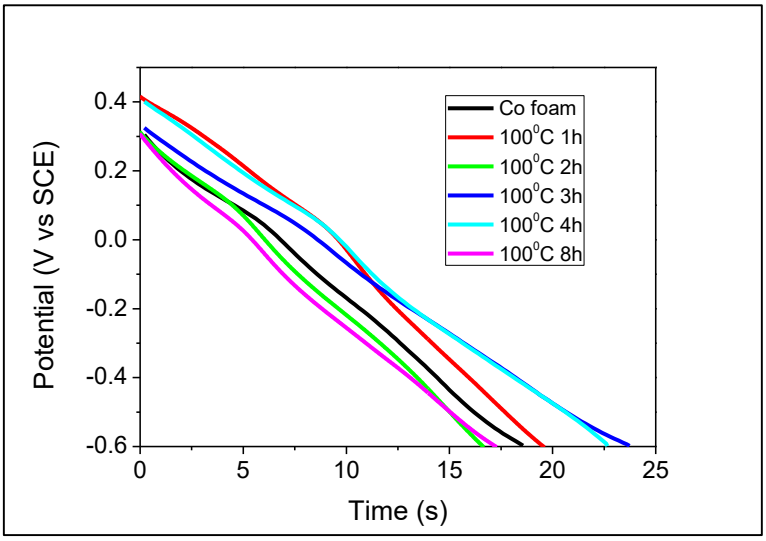

Figure 3.14 Galvanostatic discharge curves of Co nanofoams treated at 100^{0}C for different times at 1 Ag^{-1}

3.3 Effect of Chemical oxidation

Co nanofoams were chemically treated with H_2O_2 of different concentrations, ranging from 5% to 20%, for different times from 1 hour to 24 hours as explained in section 2.1.3. Electrochemical performance was tested with cyclic voltammetry and galvanostatic charge discharge. Measurements are presented in Figure 3.16. Cyclic voltammograms show a remarkable increase of the area under the CV curve compared to the untreated Co nanofoam which ensures capacitance increase. The voltammograms show faradaic redox response. In the positive potential region, the response is more resistive compared to the negative potential region.

Accordingly, galvanostatic discharge curves of chemically treated Co nanofoams exhibit a notable increase in the discharge time compared to the Co nanofoam. The discharge curves show faradaic response due to some intercalation processes.

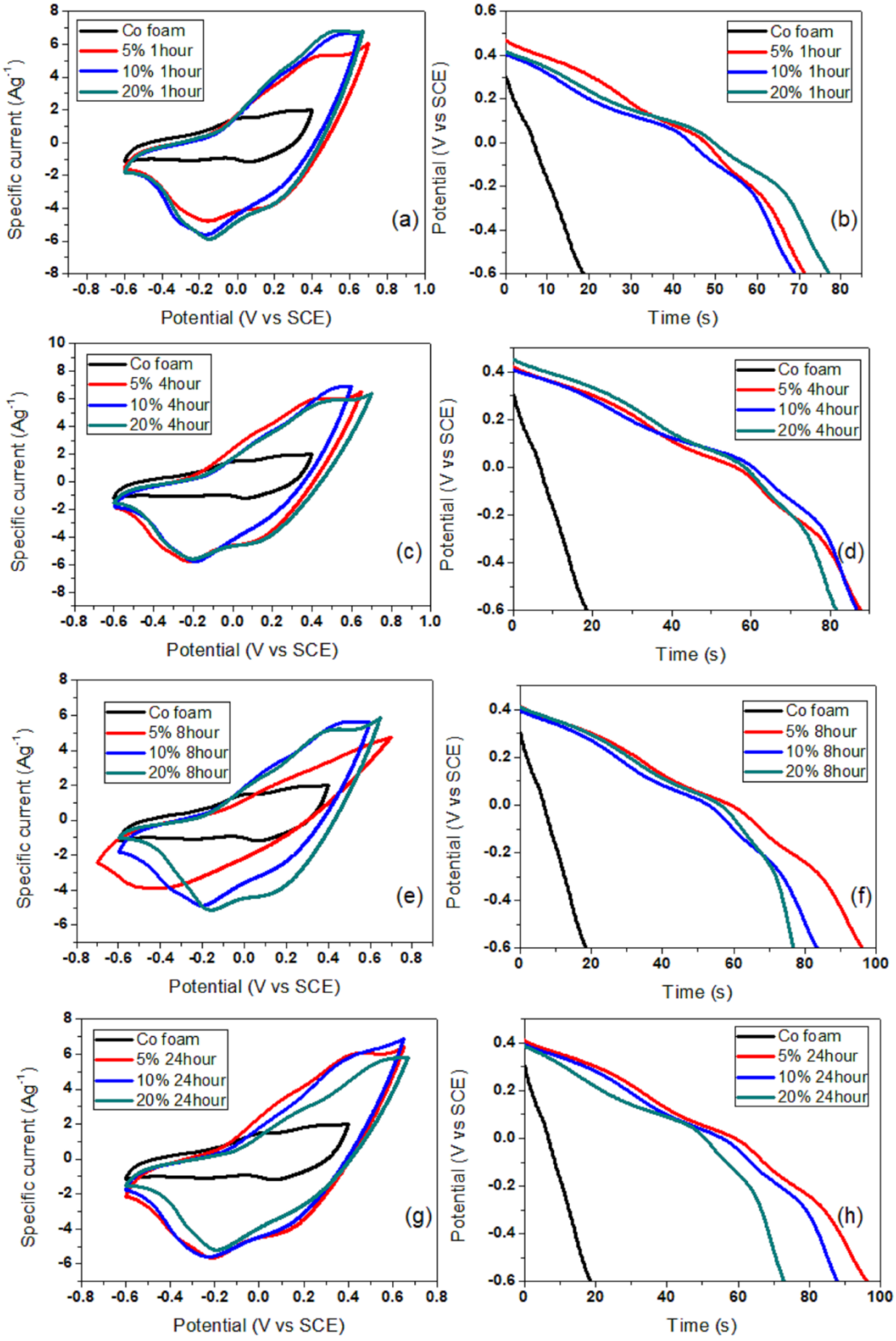

Figure 3.15 Cyclic voltammograms of Co nanofoams chemically treated with H_2O_2 of different concentrations for different times of (a) 1 hour, (c) 4 hours, (e) 8 hours, (g) 24 hours at 50 mVs^{-1} & galvanostatic charge discharge curves (b) 1 hour, (d) 4 hours, (f) 8 hours, (h) 24 hours at 1 Ag^{-1}

The effect of the concentration of H_2O_2 and treatment times on capacitance is displayed on Figure 3.17 where the specific capacitance of the treated nanofoams at $1Ag^{-1}$ are presented. The specific capacitances of chemically treated nanofoams (66-93 Fg^{-1}) are remarkably higher than the specific capacitance of Co nanofoam as shown in Table 3.1. The specific capacitance of the nanofoams treated in 5% H_2O_2 for 1 hour is 66.8 Fg^{-1} which is 228% greater than the specific capacitance of Co nanofoam (20.4 Fg^{-1}). As the treatment time increases, the specific capacitance increases for the low concentration solution (5% H_2O_2). The specific capacitance of nanofoams treated in 5% H_2O_2 for 24 hours is 95.2 Fg^{-1} which is 42% higher than the nanofoams treated in 5% H_2O_2 for 1 hour. For treatment with higher concentration of H_2O_2 (20% in this case), the specific capacitance is almost independent of the treatment time. Nanofoams treated in different concentration for 1 hour show an increase in the capacitance with the increase in concentration, while for 24 hours treatment time, the increase in concentration causes decrease in capacitance. Specific capacitance of nanofoams treated with 20% H_2O_2 for 24 hours is 73.6 Fg^{-1} which is 22% lower compared to the nanofoams treated with 5% H_2O_2 for 24 hours.

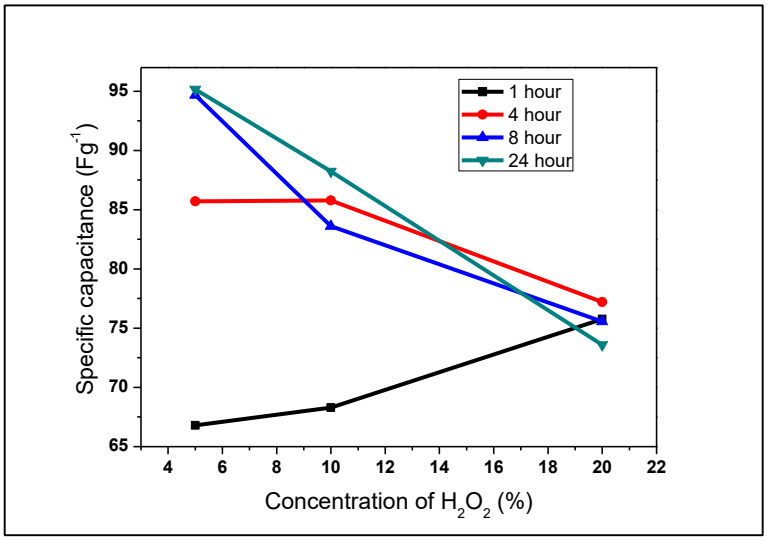

Figure 3.16 Specific capacitances of Co nanofoams chemically treated with H_2O_2 of different concentrations for different times at $1Ag^{-1}$

Overall treatment with H_2O_2 of higher concentration for longer times has worse impact compared to treatment with H_2O_2 of lower concentration. At lower concentration, the surface of the Co nanofoam comes in the contact of the oxidant that results in oxidation and activation of the surface. Increase in treatment time at lower concentration causes the oxidation of the bulk leading to higher specific capacitance. While the oxidation of the nanofoam with H_2O_2 of higher concentration may degrade the nanofoam morphology leading to the decrease in the capacitive response. This oxidation process may drastically change the structure and phase when nanofoams are exposed at increased concentrations for longer times as H_2O_2 is a very strong oxidant. Comparing all the effects of H_2O_2 concentration and treatment time, treatment with 5% H_2O_2 for 24 hours is considered as the best chemical treatment condition.

3.3.1 Physico-chemical characterization

To assess the physico-chemical properties of best chemically treated nanofoam with 5% H_2O_2 for 24 hours, SEM and XRD measurements were carried out. Figure 3.18 represents the SEM image of Co nanofoam, chemically treated with 5% H_2O_2 for 24 hours at two magnifications. The microscopic image illustrates the highly porous honeycomb like morphology identical to the Co nanofoam. The channels connecting the regular and irregular holes are increased in number for the treated nanofoams compared to the untreated one, which accounts for higher surface area and more accessible active sites for the electrolyte ions.

The XRD results in Figure 3.19 show that the intensity of peak corresponding to (111) plane of the face-centred cubic cobalt (ICDD-00-001-1259) increases compared to untreated cobalt foam, which means that the crystal (111) plane size increases when treated with 5% H_2O_2 for 24 hours. No significant changes are visible for (200) plane. No planes of cobalt oxides are seen which probably may because of the poor crystallinity of the phase formed. Therefore the XRD signals detected are from the bulk of the foam. So the oxidation due to the chemical treatment is limited to the surface only.

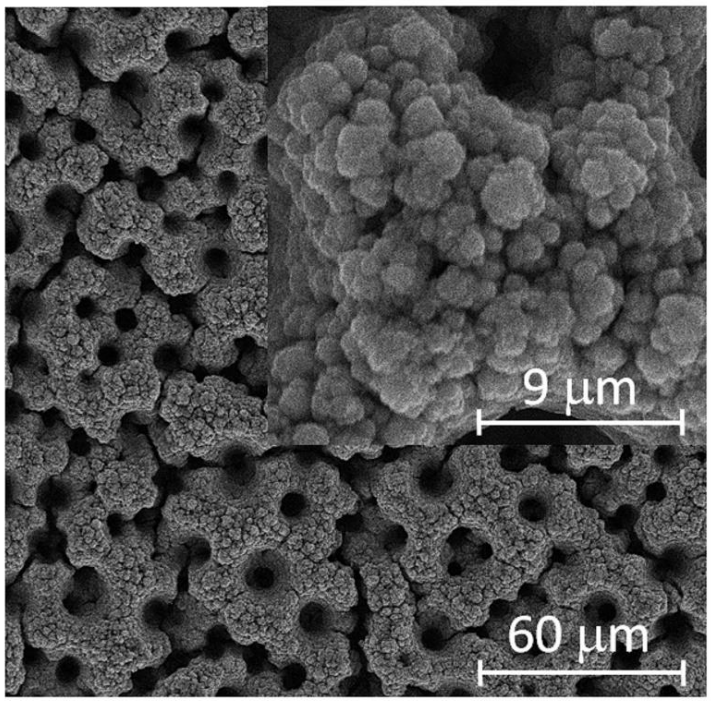

Figure 3.17 SEM image of Co nanofoam chemically treated with 5% H_2O_2 for 24 hours at 400× and 3000× magnifications (inset)

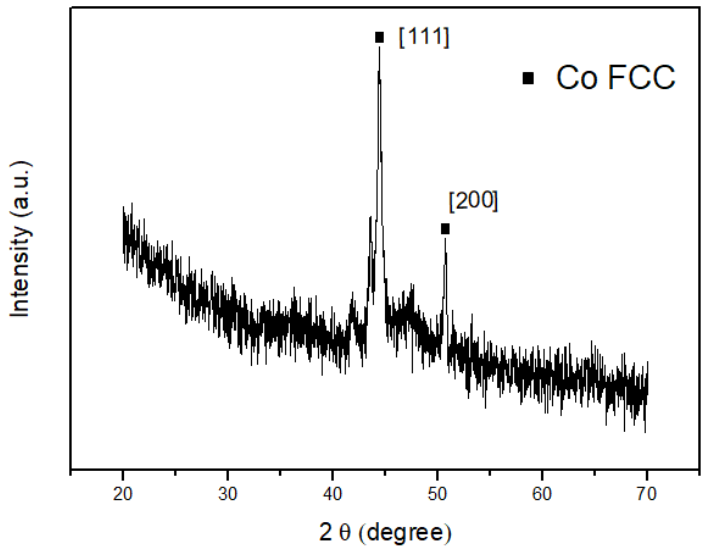

Figure 3.18 XRD spectrum of Co nanofoam chemically treated with 5% H_2O_2 for 24 hours compared with untreated Co nanofoam

3.3.2 Electrochemical characterization

Cyclic voltammetry and galvanostatic charge discharge measurements of best chemically treated nanofoam with 5% H_2O_2 for 24 hours were carried out for the electrochemical characterization. The voltammograms at different scan rates (20 mVs^{-1} - 100 mVs^{-1}) are shown in Figure 3.20. More faradaic dominated voltammograms are seen with anodic and cathodic peaks at lower scan rates. The increase of the scan rate results in the increase of the area under the voltammetry curve which accounts for increased charge storage. However, with the increase of the scan rates the response becomes resistive due to weak electrode-electrolyte interaction.

The discharge curves shown in Figure 3.21 indicate that the increase in current density from 1 Ag^{-1} to 2 Ag^{-1} causes about 70% decrease in discharge time which results a capacitance decrease of 24% from 93.9 Fg^{-1} to 70.6 Fg^{-1}. The response is more faradaic dominated, so specific capacity of the electrode was calculated at 1 Ag^{-1} and 2 Ag^{-1} as 26.1 mAh g^{-1} and 19.6 mAh g^{-1}, respectively. The increase of about ten folds in the current density causes a decrease in the discharge time from about 93 sec to about 2 sec, leading to a capacity decrease of only ~33% to 17.6 mAh g^{-1}. This indicates the good rate capability of the chemically treated Co nanofoam.

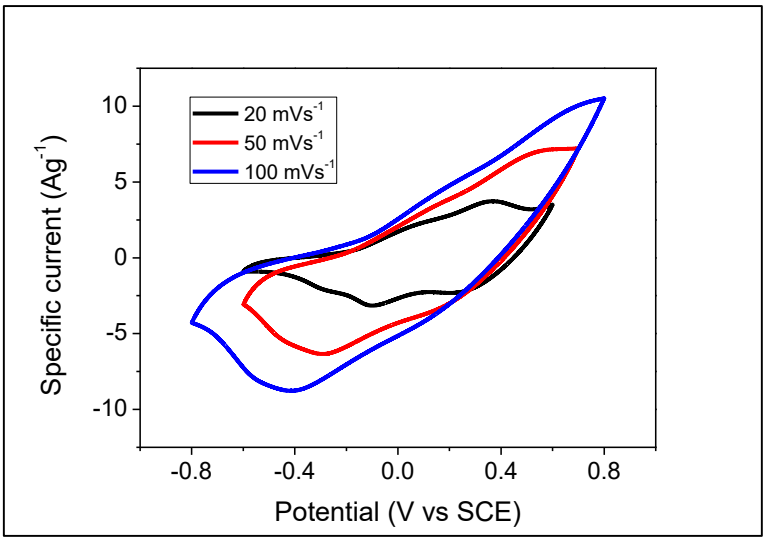

Figure 3.19 Cyclic voltammogram of Co nanofoams treated with 5% H_2O_2 for 24 hours at different scan rates

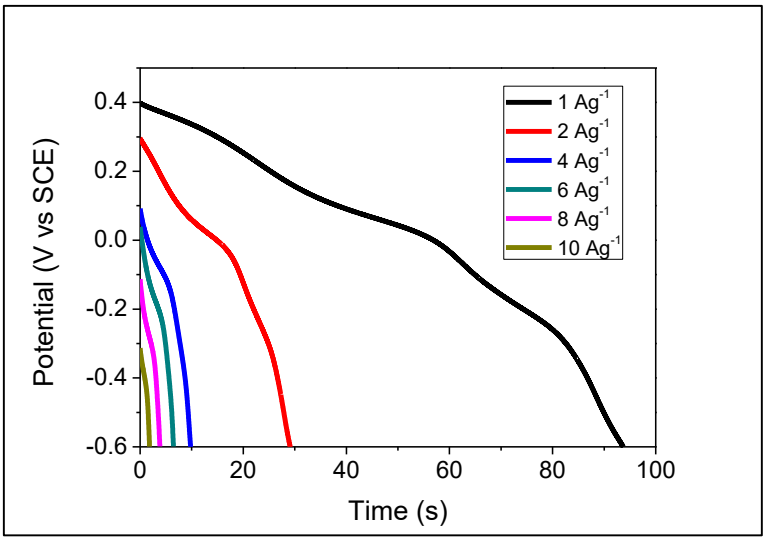

Figure 3.20 Discharge curves of Co nanofoams treated with 5% H_2O_2 for 24 hours at different current densities

Comparison of the response of chemically treated nanofoams (5% H_2O_2 for 24 hours) with untreated cobalt nanofoam are shown in Figure 3.22 and Figure 3.23. The voltammograms (Figure 3.21) at 50 mVs^{-1} show a significant increase in area under the curve for the chemically treated sample with 5% H_2O_2 for 24 hours compared to the cobalt nanofoam. This accounts for the remarkable increase of the capacitance due to this treatment. The galvanostatic discharge curves in Figure 3.23 substantiate the findings of the voltammograms. Specific capacitance at $1Ag^{-1}$ indicate an increase of about 360% from 20.4 Fg^{-1} to 93.9 Fg^{-1} after treatment with specific capacity of 26.1 mAh g^{-1}. Cycling stability (Figure 3.24) increases when the Co nanofoam is chemically treated (5% H_2O_2 for 24 hours), from 5% to about 60% after 2000 cycles of charge discharge.

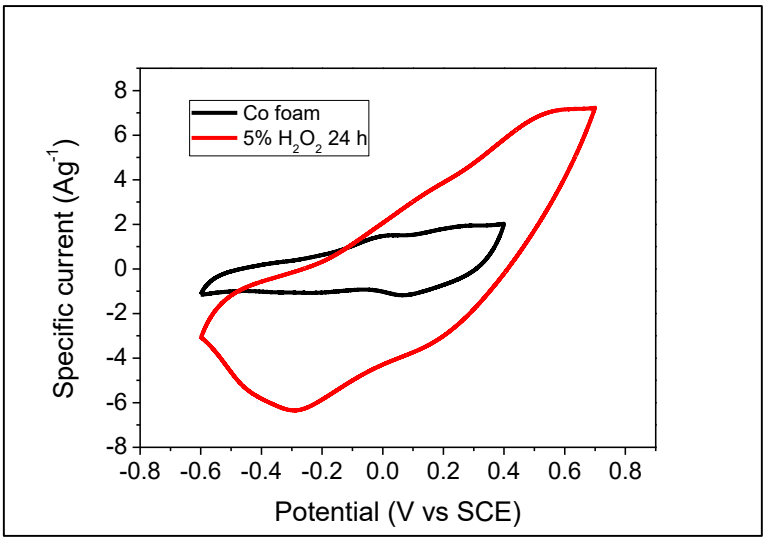

Figure 3.21 Comparison of voltammograms of as prepared Co nanofoam and of Co nanofoam chemically treated with 5% H_2O_2 for 24 hours at 50 mVs^{-1}

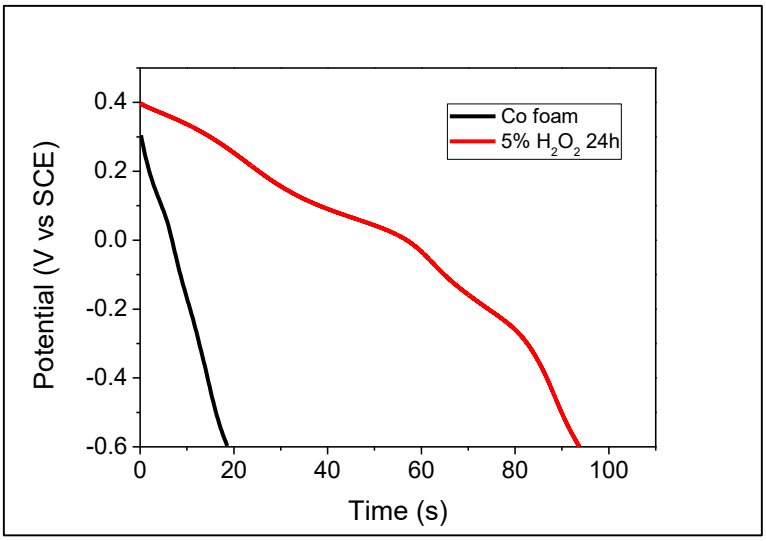

Figure 3.22 Comparison of discharge curves of as prepared Co nanofoam and of Co nanofoam chemically treated with 5% H_2O_2 for 24 hours at 1 Ag^{-1}

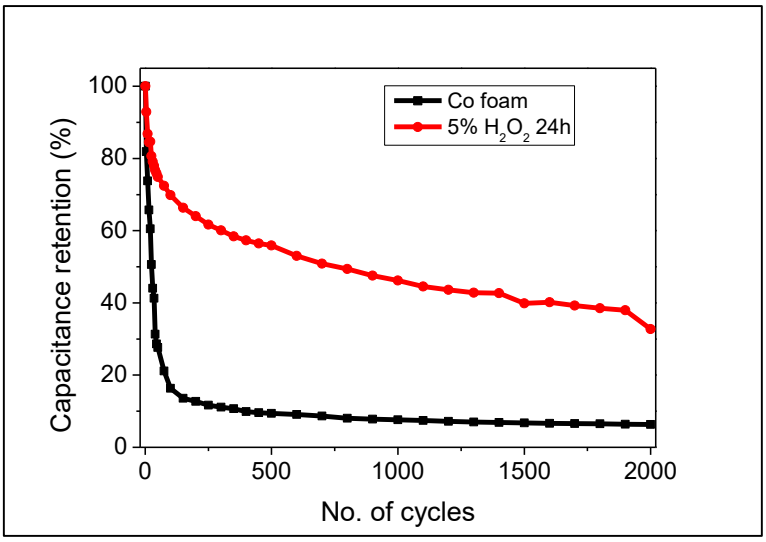

Figure 3.23 Cycling stability curves of as prepared Co nanofoam and of Co nanofoam chemically treated with 5% H_2O_2 for 24 hours during 2000 cycles

3.4 Effect of polarization

The nanofoams were polarized at 0.4 V and 1.1 V in 1M KOH solution to evaluate the effect of polarization on the electrochemical performance of the Co nanofoam. After polarization, the electrochemical performance was studied by cyclic voltammetry and galvanostatic charge discharge. The voltammograms obtained at 50 mVs^{-1} in the potential range from -0.6 V to 0.4 V are shown in Figure 3.25 demonstrate that the samples polarized at 0.4 V exhibit similar response to the Co nanofoam. The specific capacitance decreases when the electrode is polarized at 1.1 V. However, the discharge curves (Figure 3.26.) obtained at 1 Ag^{-1} show higher discharge performance when the electrode was polarized at 0.4 V compared to the Co nanofoam. In case of polarization of the electrode at 1.1 V, no significant change in discharge performance is observed compared to the Co nanofoam. This difference in performance may be due to the formation of a polarized oxide layer at the Co nanofoam surface causing activation when polarized at 0.4 V. However, polarization at a higher potential may degrade the foam or the adhesion to the substrate and foam became weak leading to decreased capacitance.

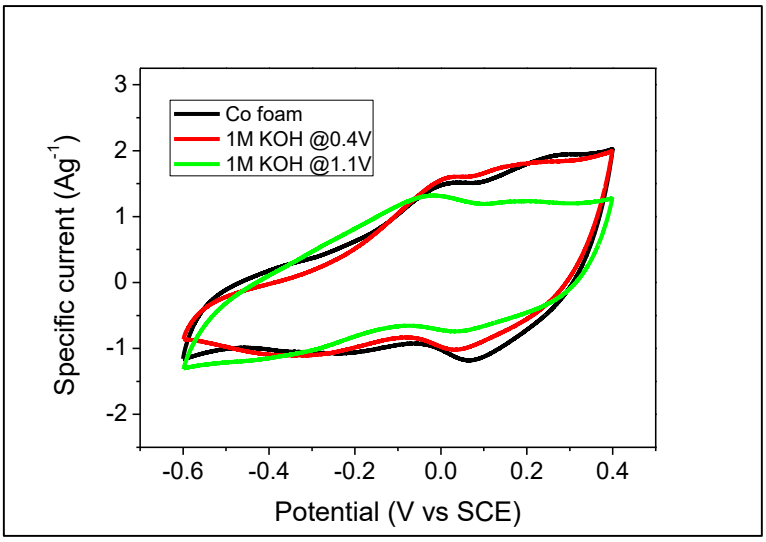

Figure 3.24 Cyclic voltammograms of polarized Co nanofoams and as prepared Co nanofoam at 50 mVs^{-1}

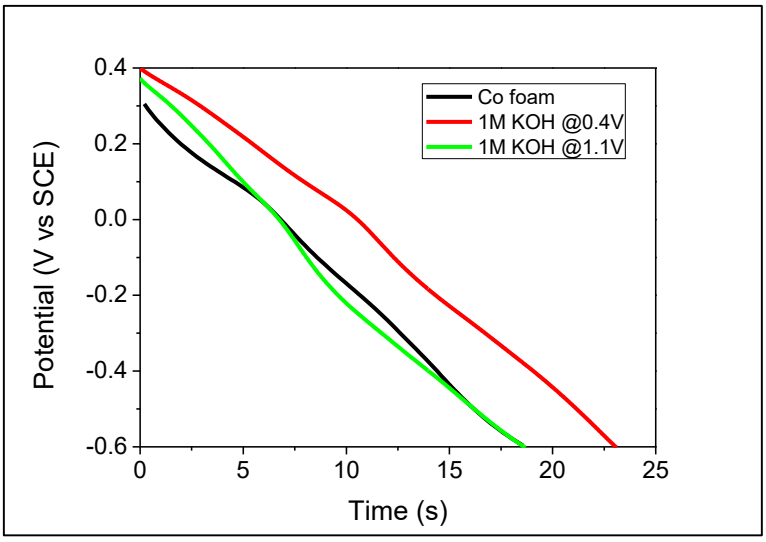

Figure 3.25 Galvanostatic discharge curves for polarized nanofoams and as prepared Co nanofoam at $1Ag^{-1}$

3.5 Effect of electrolyte concentration

3.5.1 Physico-chemical characterization

The physico-chemical properties for the samples electrochemically tested with KOH of different concentrations were analysed by SEM and XRD for comparison. The SEM image of samples tested with 0.1 M, 1 M and 4 M KOH at two different magnifications are shown in Figure 3.27. The SEM image of sample tested with low concentration (0.1 M) of KOH shows the honeycomb like morphology with

cauliflower like agglomerates. Porous holes that are connected by channels are seen in the image, being identical to the Co nanofoam. As the electrolyte concentration increases to 1 M, small spike like features are seen in the cauliflower agglomerates. For the higher KOH concentration (4 M), a significant change in the morphology is seen. The surface of the nanofoam is covered with some cloudy layer which makes the cauliflower like nanostructures more agglomerated. The porosity clearly decreases leading to lower surface area.

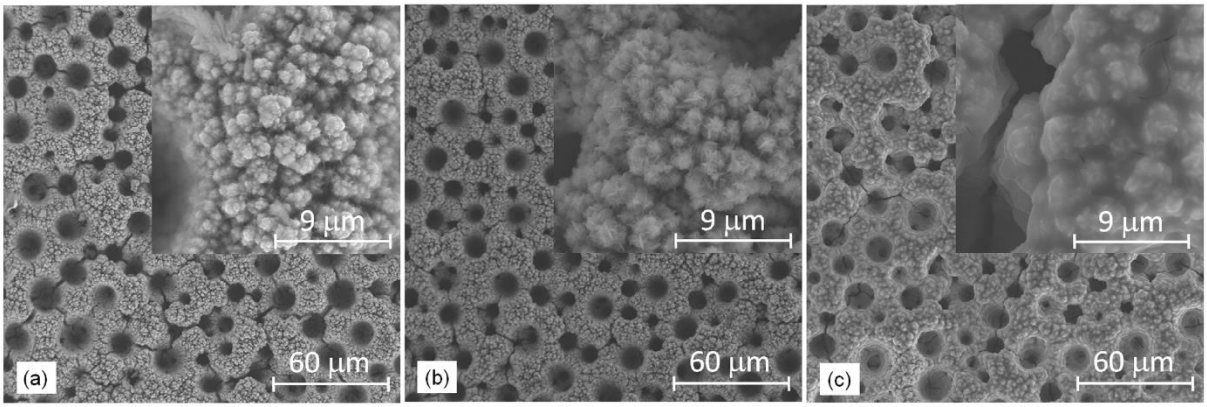

Figure 3.26 SEM images of Co nanofoams tested in (a) 0.1 M KOH; (b) 1 M KOH; (c) 4 M KOH at 400× magnification and 3000× magnification (inset)

The XRD images for samples tested with different concentrations of KOH is shown in Figure 3.28 for comparison with untreated Co nanofoam. While tested with 0.1 M KOH, no significant change in the planes are seen after the measurement. Electrochemical measurements with higher concentration of KOH (1 M and 4 M) shows significant changes in the phases present in the nanofoam. After measurements in 1M, six different planes (100), (011), (012), (110), (111) and (200) of hexagonal closed packed $Co(OH)_2$ (ICDD 01-089-8616) appear at 32.3^0, 37.9^0, 51.4^0, 57.9^0, 61.4^0, 67.9^0 and 69.5^0, respectively. The peaks present at 43.5^0, 44.3^0, and 50.5^0 correspond to stainless steel (substrate). After testing with 4 M KOH, the planes of $Co(OH)_2$ HCP are found as observed for 1 M KOH with peaks corresponding to stainless steel substrate as well.

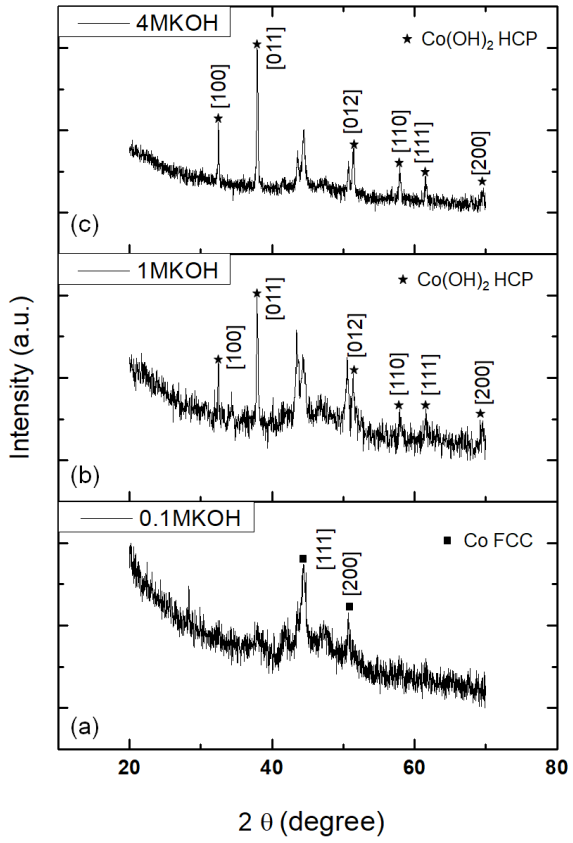

Figure 3.27 XRD spectrum of Co nanofoams tested in (a) 0.1 M KOH; (b) 1 M KOH and (c) 4 M KOH,

3.5.2 Electrochemical characterization

The effect of electrolyte concentration during the electrochemical measurements were tested with cyclic voltammetry and galvanostatic charge discharge measurements. The cyclic voltammetry analysis was carried out with different concentrations of KOH (0.1 M - 4 M) at 50 mVs^{-1} and are presented in Figure 3.29. The voltammograms show that the performance of the Co foam is pseudocapacitive with high resistance in the positive potential range when measured with lower concentrations of KOH (0.1 M - 0.2 M). At lower concentration, less ions are in the electrolyte to reach all the active sites. As the concentration of KOH increases to 0.5 M, the response exhibits combination of pseudocapacitive and intercalation partial-redox type feature. The surface area under the voltammetry curve decreases, and more defined peaks appear as the electrolyte concentration increases from 0.5 M to 2 M. The voltammograms obtained in 4 M KOH display a faradaic redox response with a pair of well-defined redox peaks, but with a much smaller area under the voltammograms indicating faradaic dominated battery like behaviour. These voltammetry profiles substantiate the morphological change observed from the Figure 3.27 showing that a decrease of surface area leads to lower specific capacitance.

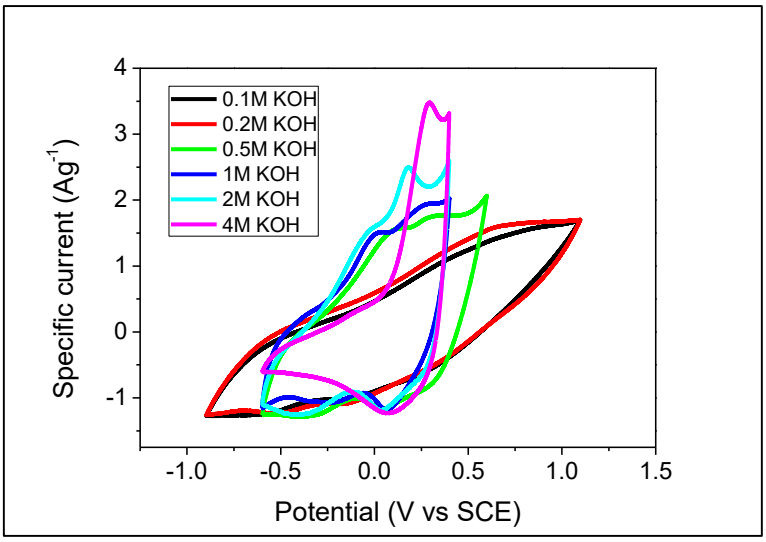

Figure 3.28 Cyclic voltammograms of Co nanofoams tested in KOH of different concentrations at 50 mVs^{-1}

The discharge curves for different concentrations of KOH (0.1 M – 4 M) at 1 Ag^{-1} are presented in Figure 3.30. The curves indicate the same features as seen for the voltammograms in Figure 3.29. For very low concentrations of electrolyte, the response is almost linear representing a pseudocapacitive behaviour. At concentrations between 0.5 M to 2 M, more waves appear along with the linear response that can be explained by a combination of pseudocapacitance with intercalation type charge storage mechanism. In 4 M KOH, the discharge curve indicates a faradaic response[46].

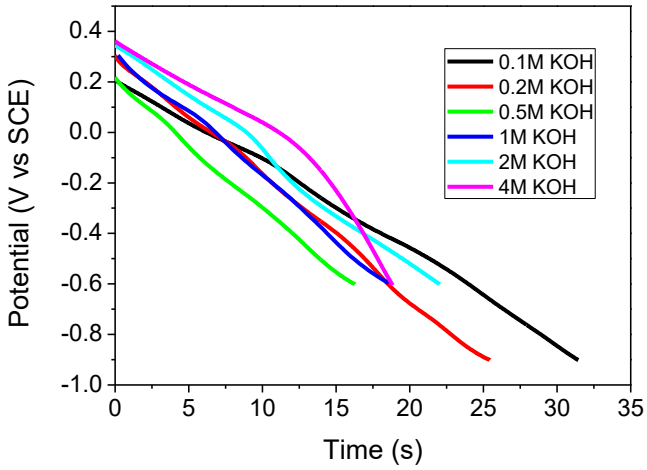

Figure 3.29 Discharge curves of Co nanofoams tested in KOH of different concentrations at $1Ag^{-1}$

3.6 Electrochemical cell set up

To assess the performance of the Co nanofoam and treated Co nanofoam, symmetric and asymmetric cells were assembled. For the asymmetric cell, carbon was used as negative electrode. The electrochemical performance of the cells was studied using cyclic voltammetry, galvanostatic charge discharge and cycling stability measurements.

3.6.1 Symmetric cell with Co nanofoam

Symmetric cell was set up with the produced Co nanofoam. Before assembling, Co nanofoam was stabilized in 1 M KOH by the imposition of 20 cyclic voltammetry cycles. The electrochemical performance was assessed with cyclic voltammetry in 1 M KOH, with scan rates ranging between 20 mVs^{-1} and 100 mV^{-1} in a potential range from 0 V to 1.7 V. The voltammograms presented in Figure 3.31 show that at potential lower than 0.8 V, specific current is very low indicating poor charge storage ability. At potential higher than 0.8 V, a pseudocapacitive response with superficial intercalation is observed. Galvanostatic charge discharge measurements were carried out for a range of current densities (0.1 Ag^{-1} - 1 Ag^{-1}). The discharge curves (Figure 3.32) also indicate similar response with resistive and poor charge storage ability as observed in the voltammograms. With ten-fold increase of the current density (0.1 Ag^{-1} - 1 Ag^{-1}), 51% decrease of the specific capacitance from 1.2 Fg^{-1} to 0.6 Fg^{-1} is seen. The cycling stability was measured calculating the capacitance retention for 2000 cycles. The plot in Figure 3.33 indicates that the cell retains about 65% of capacitance by the end of 2000 cycles which reveals the poor stability of the material[7].

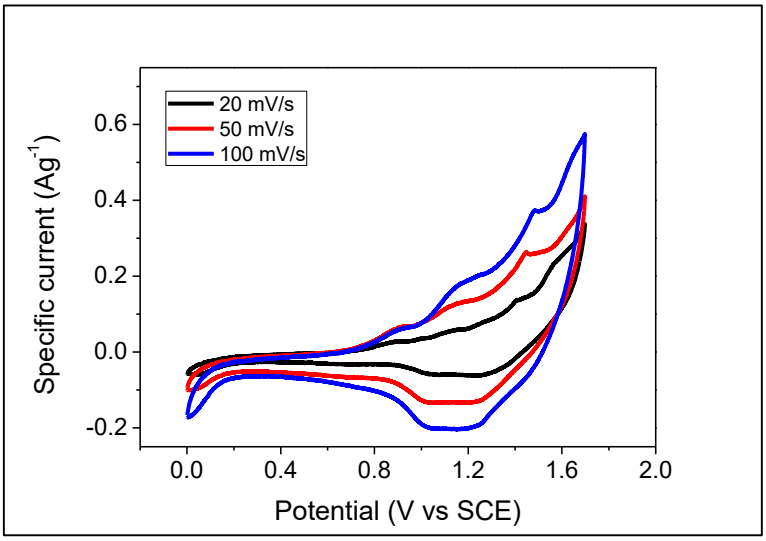

Figure 3.30 Cyclic voltammograms of symmetric cell with stabilized Co nanofoam at different scan rates

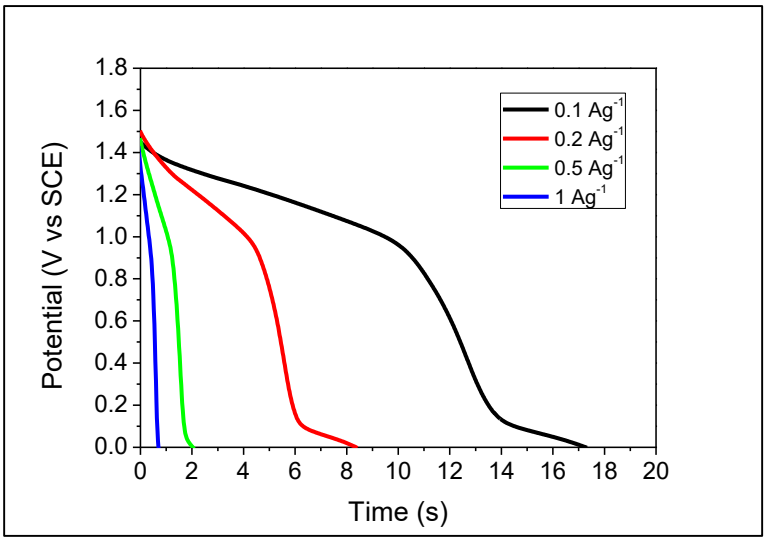

Figure 3.31 Galvanostatic discharge curves of symmetric cell with stabilized Co nanofoam at different current densities

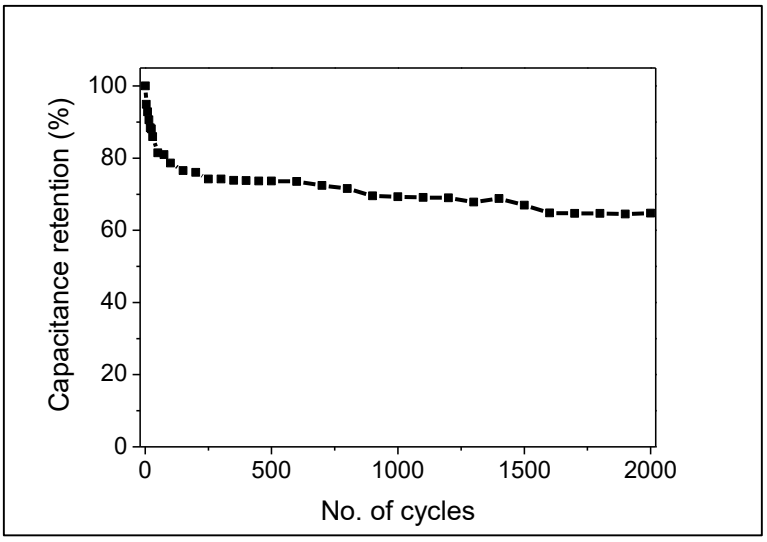

Figure 3.32 Cycling stability of symmetric cell with stabilized Co nanofoam during 2000 cycles

3.6.2 Symmetric cell with chemically treated Co nanofoam (5% H_2O_2 24h)

Co nanofoam treated with 5% H_2O_2 for 24 hours was used as electrodes to assemble a symmetric cell. Before assembling, the treated Co nanofoam was stabilized with 10 potential cycles. The electrochemical performance was tested by cyclic voltammetry and galvanostatic charge discharge. The voltammograms (Figure 3.34) analysed at different scan rates (20 mVs^{-1} – 200 mVs^{-1}) reveal faradaic dominating responses. When the scan rate increases the anodic and cathodic peaks shift to more negative and positive direction, which indicates the quasi-reversible nature of the redox reactions and fast reactions occurring at the electroactive material - electrolyte interface[48]. The galvanostatic discharge curves in Figure 3.35 at different current densities (0.1 Ag^{-1} - 2 Ag^{-1}) exhibit a combination of intercalation

partial redox and faradaic processes. The discharge time at 0.1 Ag^{-1} corresponds to specific capacity of 10.5 $mAhg^{-1}$. For 20-fold increase in current density, specific capacity decreases about 51% presenting a value of 6 $mAhg^{-1}$ at 2 Ag^{-1}. The cycling stability measurement of this cell show fast cycling degradation (Figure 3.36). The electrode active material may have faced detachment from the substrate after 300 cycles which causes the unstable response.

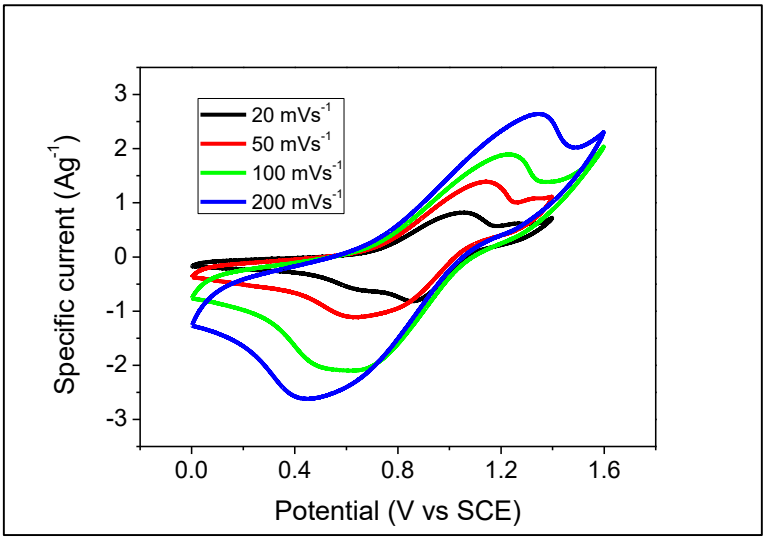

Figure 3.33 Cyclic voltammograms of symmetric cell with chemically treated Co nanofoam (5%H_2O_2 24h) at different scan rates

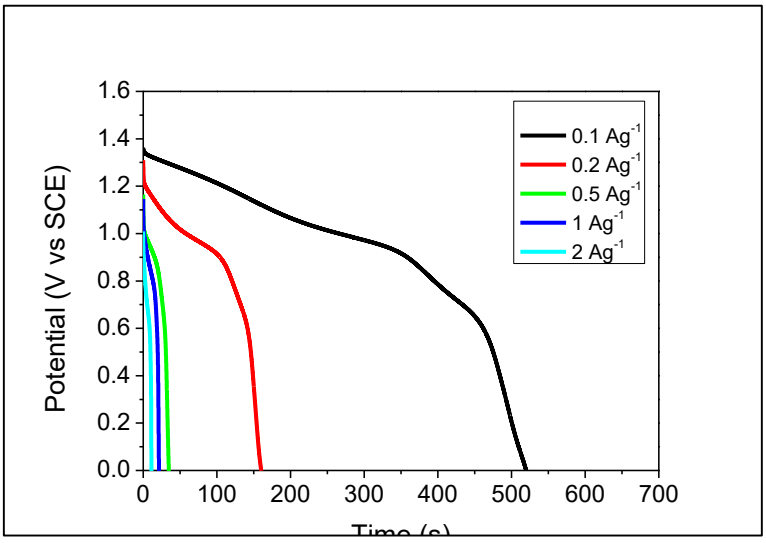

Figure 3.34 Galvanostatic discharge curves of symmetric cell with chemically treated Co nanofoam (5% H_2O_2 24h) at different current densities

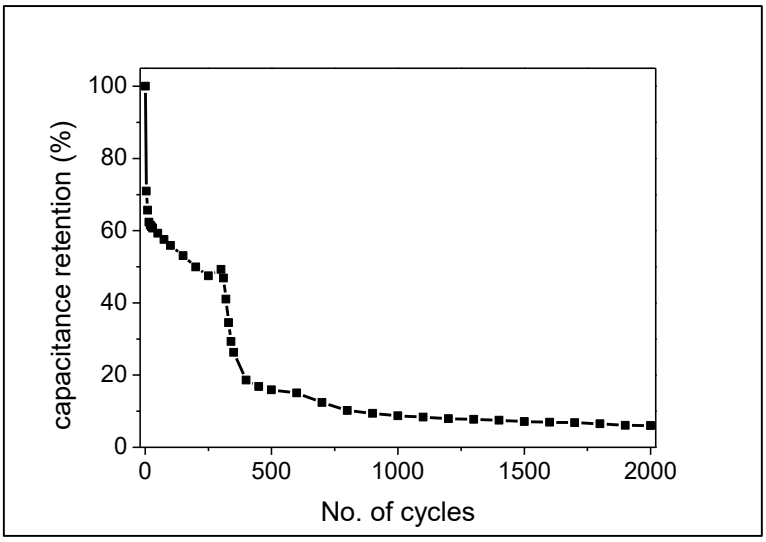

Figure 3.35 Cycling stability curve of symmetric cell with chemically treated Co nanofoam (5%H_2O_2 24h) during 2000 cycles

3.6.3 Carbon electrode testing

Carbon was used as the negative electrode for assembling an asymmetric cell. The electrochemical performance of carbon was evaluated with cyclic voltammetry, galvanostatic charge discharge and cycling stability measurements. The cyclic voltammetry of the carbon electrode was measured for a range of scan rates (10 mVs^{-1} - 100 mVs^{-1}) in the potential range from -0.9 V to 0.2 V. The voltammograms (Figure 3.37) represent no peaks, hence, the charge storage occurs via electrostatic phenomenon[46] as expected for carbon materials in section 1.4.1. Voltammograms show increased resistance at higher scan rates. The galvanostatic charge discharge analysis was carried out for 1 Ag^{-1} to 10 Ag^{-1} current densities in a potential range from -0.9 V to 0 V. The discharge curves in Figure 3.38 represent almost linear behaviour indicating capacitive response. The specific capacitance decreases about 43% from 173 Fg^{-1} to 97 Fg^{-1} for ten-fold increase in current density from 1 Ag^{-1} to 10 Ag^{-1}, respectively. The stability of carbon was tested with 2000 charge-discharge cycles at 4 Ag^{-1} is presented in Figure 3.39. The capacitance retention was calculated from the discharge curves. The capacitance retention of carbon indicates excellent cycling stability. The reason of this high capacitance with the increase of cycling is due to the increased wettability of the carbon surface caused by soaking in the electrolyte for longer time.

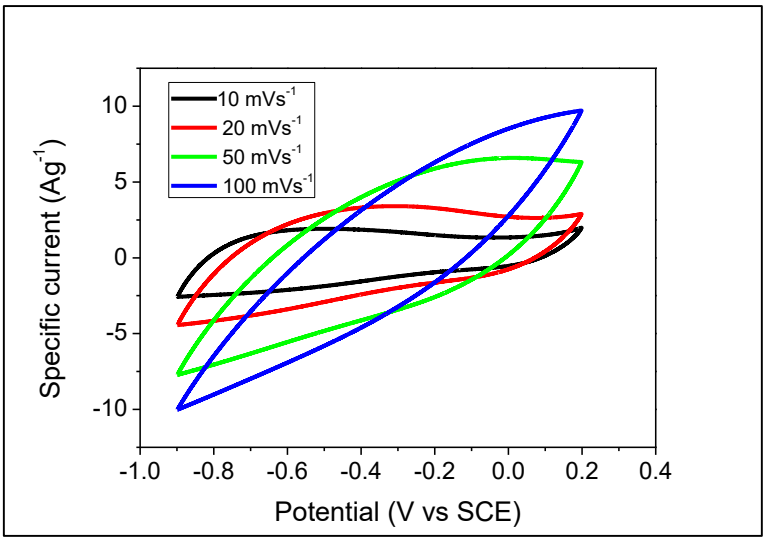

Figure 3.36 Cyclic voltammograms of carbon at different scan rates

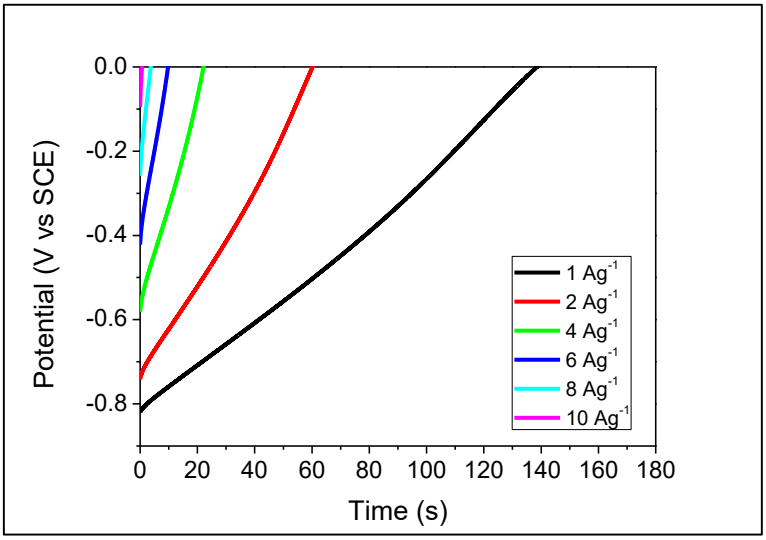

Figure 3.37 Galvanostatic discharge curves of carbon at different current densities

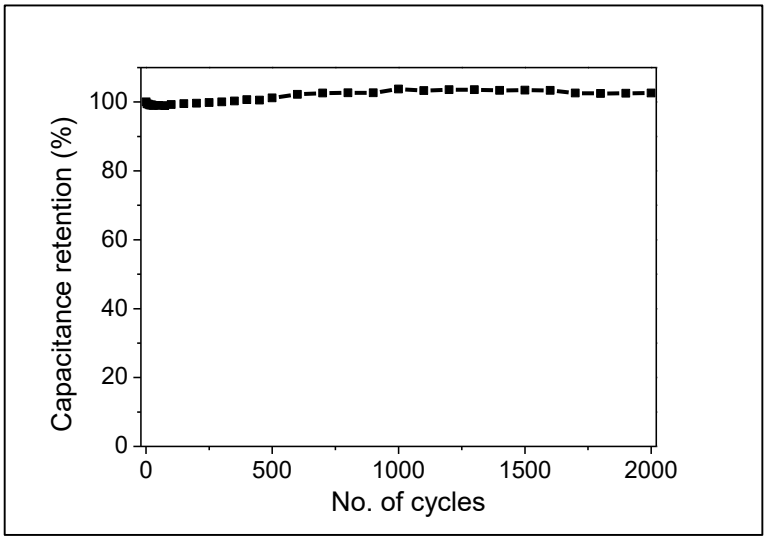

Figure 3.38 Cycling stability of carbon during 2000 cycles

3.6.4 Asymmetric cell with Co nanofoam - Carbon

Asymmetric cell was assembled with cobalt nanofoam as the positive electrode and carbon as the negative electrode. Cyclic voltammetry carried out in 1 M KOH for scan rates ranging from 10 mVs^{-1} to 50 mVs^{-1} are shown in Figure 3.40. The absence of sharp redox peaks indicates mainly pseudocapacitive responses and poor charge storage ability and increased resistance in the potential range higher than 1.3 V is seen from the response. With increased scan rate the capacitance does not change much, representing rate stability of the cell. Galvanostatic discharge curves for current density from 0.1 Ag^{-1} to 1 Ag^{-1} (Figure 3.41) exhibit pseudocapacitive behaviour with a capacitance decrease of 50% from 4.5 Fg^{-1} to 2.3 Fg^{-1} calculated at 0.1 Ag^{-1} and 1 Ag^{-1}, respectively. The capacitance retention plot (Figure 3.42) for 2000 cycles indicate a rapid capacitance drop for the first 100 cycles, but good rate stability of the cell was observed afterwards.

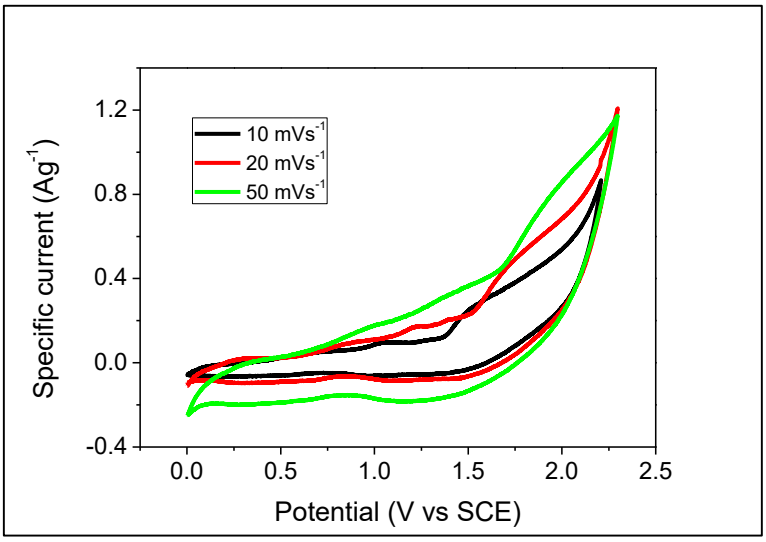

Figure 3.39 Cyclic voltammograms of asymmetric cell with Co nanofoam - carbon at different scan rates

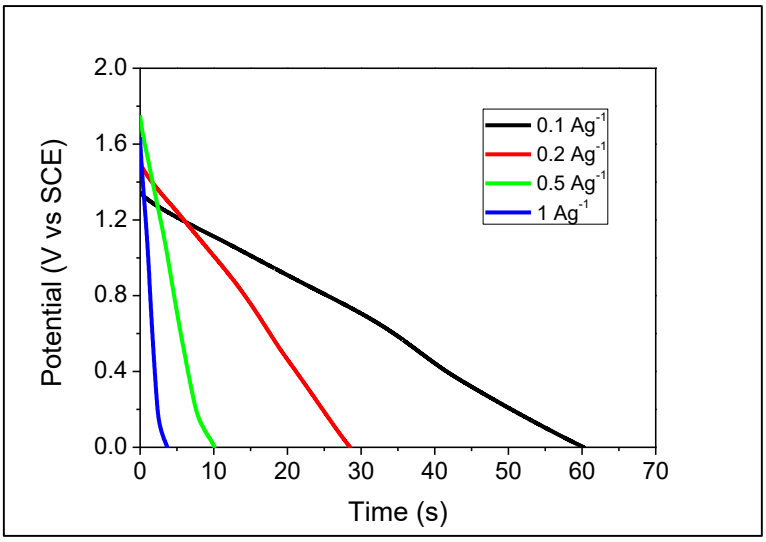

Figure 3.40 Galvanostatic discharge curves of asymmetric cell with Co nanofoam - carbon at different current densities

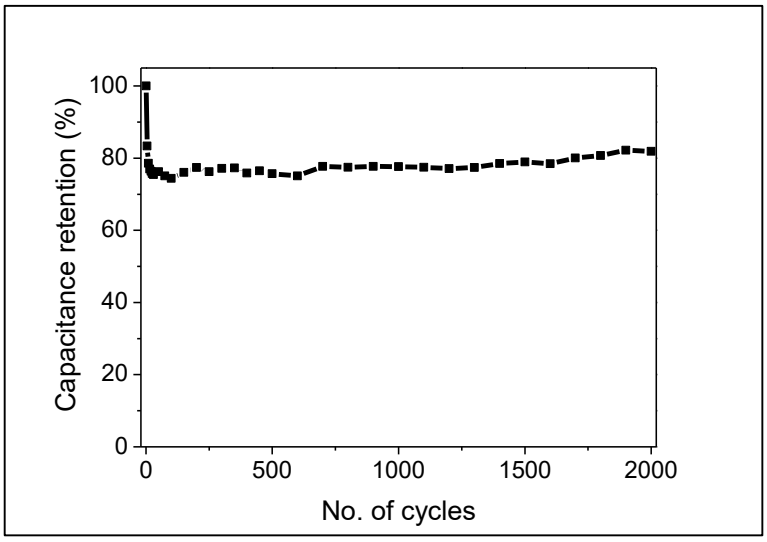

Figure 3.41 Cycling stability of asymmetric cell with Co nanofoam - carbon during 2000 cycles

3.6.5 Asymmetric cell with chemically treated Co nanofoam (5% H_2O_2 24h) - Carbon

Chemically treated Co nanofoam with 5% H_2O_2 for 24 hours was used as the positive electrode and carbon as the negative electrode to assemble an asymmetric cell. The cell was studied in 1 M KOH with cyclic voltammetry and galvanostatic charge discharge. The cycling stability was also measured. The voltammograms in Figure 3.43 measured for different scan rates indicate pseudocapacitive response combined with an intercalation type redox process. The increase in scan rates show some resistance associated to the electrode-electrolyte interaction. Galvanostatic discharge curves (Figure 3.44) for different current densities from 0.1 Ag^{-1} to 2 Ag^{-1} corroborate the pseudocapacitive response indicating a decrease in capacitance with the current increase. The specific capacitance for 0.1 Ag^{-1} is 34.6 Fg^{-1}

which decreases only 2% to 33.9 Fg^{-1} for 20-fold increase in current to 2 Ag^{-1} indicating excellent rate stability. The cell shows specific energy of 7.8 Wh kg^{-1} for specific power of 63.6 kW kg^{-1} which is maintained remarkably even at high specific power of 1288 kW kg^{-1} (Figure 3.45). This denotes excellent electrochemical stability of the cell. The capacitance retention plot (Figure 3.46) shows only 10% capacitance lose after 2000 cycles which reveals good cycling stability.

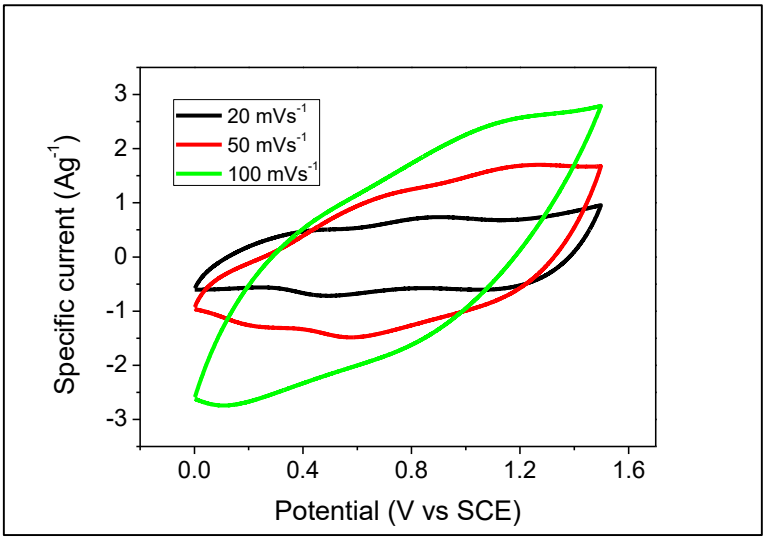

Figure 3.42 Cyclic voltammograms of asymmetric cell with chemically treated Co nanofoam (5%H_2O_2 24h) - carbon at different scan rates

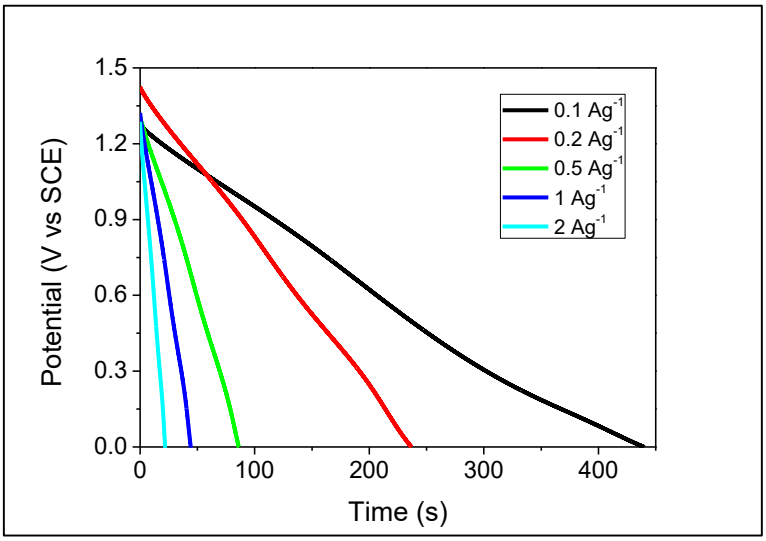

Figure 3.43 Galvanostatic discharge curves of asymmetric cell with chemically treated Co nanofoam (5%H_2O_2 24h) - carbon at different current densities

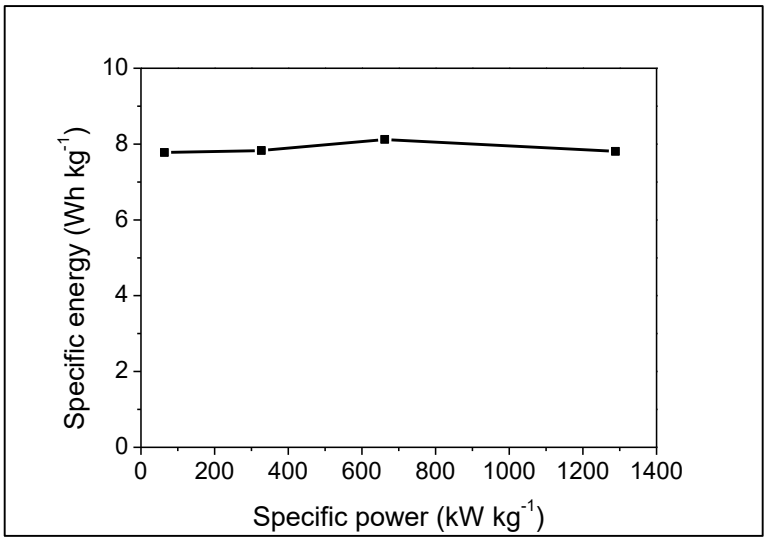

Figure 3.44 Ragone plot of asymmetric cell with chemically treated Co nanofoam (5% H_2O_2 24h) - carbon

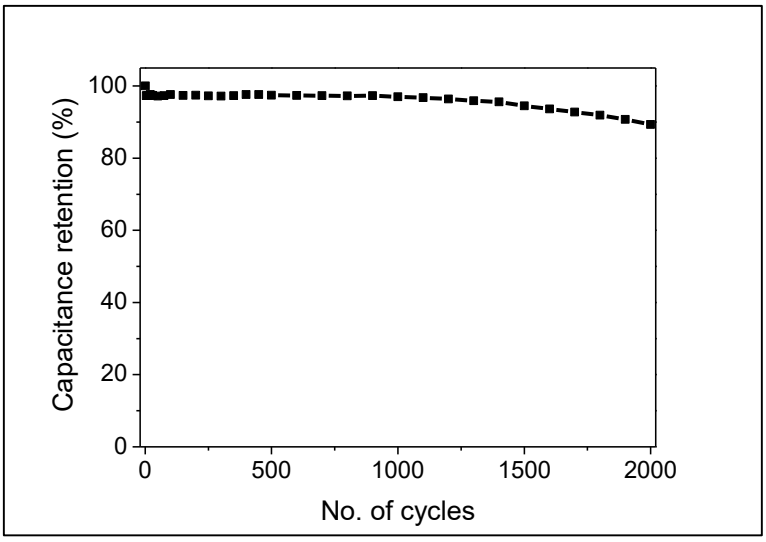

Figure 3.45 Cycling stability curve of chemically treated Co nanofoam (5%H_2O_2 24h) - carbon asymmetric cell during 2000 cycles

Chapter 4

Conclusions

The objective of the present work was to develop a metallic cobalt nanofoam by DHBT electrodeposition method to form honeycomb like morphologies with cauliflower agglomerates and to evaluate the electrochemical performance of the nanofoams. Further oxidation of the nanofoams by different oxidation methods to tune the electrochemical properties and to evaluate the electrochemical potential of the functionalized nanofoams as supercapacitor electrode material were carried out in this research work.

The Co nanofoam was electrodeposited by DHBT method on stainless steel substrates. The morphology of the nanofoam was characterized by SEM and the expected honeycomb like morphology with cauliflower agglomerates was well defined, implying an increased surface area. The XRD results showed the presence of (111) and (200) planes of face-centred cubic cobalt. Cyclic voltammetry and galvanostatic charge discharge measurements in 1M KOH revealed a combination of pseudocapacitive and intercalation redox charge storage mechanism in the nanofoam with 20.4 Fg^{-1} specific capacitance at 1 Ag^{-1} current density. However, the as formed Co nanofoam exhibited very poor cycling stability.

Thermal treatment of the cobalt nanofoam at different temperatures revealed that at temperature lower than 250^0C, both physico-chemical and electrochemical performance was not very different from the

untreated nanofoam. Treatment at temperatures higher than 250^0C decreases significantly the capacitance. XRD results after treatment at 400^0C reveal the presence of seven different planes of face-centred cubic Co_3O_4.

Chemical oxidation of the Co nanofoam with 5%H_2O_2 for 24 hours exhibited remarkable electrochemical performance compared to the metallic cobalt nanofoam due to the formation of $Co(OH)_2$ since this is the electrochemically active phase in 1 M KOH. The response becomes dominated by faradaic processes after treatment. The specific capacity increased about 360% from 5.7 $mAhg^{-1}$ to 26.1 $mAhg^{-1}$ at 1 Ag^{-1}. The cycling stability improves after the treatment. The surface area of the nanofoam increases as confirmed by SEM results and the XRD peaks reveal that the (111) plane of Co FCC becomes more defined after chemical treatment in 5% H_2O_2 for 24 hours.

Co nanofoams were polarized at 0.4 V and 1.1 V to evaluate the effect of polarization on the electrochemical performance. No significant changes were observed due to the polarization of the nanofoam.

The concentration of the electrolyte has great impact on the performance of the Co nanofoam. KOH at very low concentration shows highly resistive pseudocapacitive response. 0.5 M – 2 M KOH shows better performance with a combination of pseudocapacitive and intercalation type behaviour and 1 M is taken as the optimum concentration for electrochemical measurements.

The potential of Co nanofoam and chemically treated Co nanofoam to use in cell were tested by fabricating symmetric and asymmetric supercapacitor cells. Co-Co symmetric cell showed a combination of pseudocapacitive and intercalation type response with 50% decrease of the specific capacitance from 1.2 Fg^{-1} to 0.6 Fg^{-1} for 0.1 Ag^{-1} to 1 Ag^{-1} respectively. The symmetric cell showed 60% capacitance retention after 2000 cycles of charge discharge which indicates poor cycling stability.

Symmetric cells comprised of chemically treated Co nanofoam (5%H_2O_2 24 hours) revealed a combination of faradaic and intercalation redox type mechanisms with a specific capacity value of 10.6 $mAhg^{-1}$ at 0.1 Ag^{-1} specific current. However, the cell showed poor cycling stability.

An asymmetric cell was set up with the Co nanofoam (stabilized in 1 M KOH with 20 cycles of cyclic voltammetry) as positive electrode and carbon as negative electrode. The carbon material used, exhibited capacitive response with excellent cycling stability. The specific capacitance for the carbon at 1Ag^{-1} current density was calculated as 173 Fg^{-1}.

Co nanofoam ($Co(OH)_2$ as electrochemically active phase) - C asymmetric cell was assembled to evaluate the performance of Co nanofoam as positive electrode for supercapacitor. The symmetric cell showed a pseudocapacitive response with increased resistance at higher potential. The specific capacitance is very low with a value of 2.3 Fg^{-1} at 1 Ag^{-1}. This asymmetric cell showed good cycling stability after 2000 cycles of charge discharge.

Chemically treated Co nanofoam (5% H_2O_2 24 hour) was used as the positive electrode and carbon material was used as the negative electrode for the asymmetric cell to be evaluated. The cell showed excellent pseudocapacitive response with 34.6 Fg^{-1} specific capacitance at 0.1 Ag^{-1} current density. The

rate stability was excellent as for 20-fold increase of current density caused only 2% decrease in the capacitance giving a value of 33.9 Fg^{-1} at 2 Ag^{-1}. The asymmetric cell also exhibited remarkable cycling stability after 2000 cycles and retained 90% of the capacitance. The cell showed specific energy of 7.8 Wh kg^{-1} at specific power of 63.6 kW kg^{-1} and no change in the specific energy was observed at high specific power of 1288 kW kg^{-1}.

To conclude, the performance of Co nanofoam chemically treated with 5% H_2O_2 for 24 hours exhibit a tremendous improvement in the electrochemical performance compared to the untreated Co nanofoam. Considering the excellent electrochemical performance and cycling stability in the asymmetric cell, the results highlight the potential of the chemically treated nanofoam as a positive electrode in asymmetric supercapacitors.

References

1. Outlook, BP Energy. 2019 edition.
2. Gallo, A. B., Simões-Moreira, J. R., Costa, H. K. M., Santos, M. M. & Moutinho dos Santos, E. Energy storage in the energy transition context: A technology review. *Renew. Sustain. Energy Rev.* **65**, 800–822 (2016).
3. Chen, G. Z. Supercapacitor and supercapattery as emerging electrochemical energy stores. *Int. Mater. Rev.* **62**, 173–202 (2017).
4. Miller, J. R. A brief history of supercapacitors. *Batter. Energy Storage Technol.* 61 (2007).
5. González, A., Goikolea, E., Barrena, J. A. & Mysyk, R. Review on supercapacitors: Technologies and materials. *Renew. Sustain. Energy Rev.* **58**, 1189–1206 (2016).
6. Saleem, A. M., Desmaris, V. & Enoksson, P. Performance Enhancement of Carbon Nanomaterials for Supercapacitors. *Journal of Nanomaterials* **2016**, (2016).
7. Chen, S.-M., Ramachandran, R., Mani, V. & Saraswathi, R. *Recent Advancements in Electrode Materials for the High-performance Electrochemical Supercapacitors: A Review*. *Int. J. Electrochem. Sci* **9**, (2014).
8. Bose, S. *et al.* Carbon-based nanostructured materials and their composites as supercapacitor electrodes. *J. Mater. Chem.* **22**, 767–784 (2012).
9. Pandolfo, A. G. & Hollenkamp, A. F. Carbon properties and their role in supercapacitors. *J. Power Sources* **157**, 11–27 (2006).
10. SIMON, P. & GOGOTSI, Y. Materials for electrochemical capacitors. in *Nanoscience and Technology* 320–329 (Co-Published with Macmillan Publishers Ltd, UK, 2009). doi:10.1142/9789814287005_0033
11. Augustyn, V., Simon, P. & Dunn, B. Pseudocapacitive oxide materials for high-rate electrochemical energy storage. *Energy Environ. Sci.* **7**, 1597 (2014).
12. Wang, G., Zhang, L. & Zhang, J. A review of electrode materials for electrochemical supercapacitors. *Chem. Soc. Rev.* **41**, 797–828 (2012).
13. Yang, X., Ma, H. & Zhang, G. Nitrogen-Doped Mesoporous Carbons for Supercapacitor Electrodes with High Specific Volumetric Capacitance. *Langmuir* **33**, 3975–3981 (2017).
14. Portet, C., Taberna, P. L., Simon, P. & Flahaut, E. Influence of carbon nanotubes addition on carbon–carbon supercapacitor performances in organic electrolyte. *J. Power Sources* **139**, 371–378 (2005).

15. Zheng, W. *et al.* Nanocellulose-mediated hybrid polyaniline electrodes for high performance flexible supercapacitors. *J. Mater. Chem. A* **5**, 12969–12976 (2017).

16. Xia, H., Shirley Meng, Y., Yuan, G., Cui, C. & Lu, L. A Symmetric RuO2/RuO2 Supercapacitor Operating at 1.6 V by Using a Neutral Aqueous Electrolyte. *Electrochem. Solid-State Lett.* **15**, A60 (2012).

17. Xiao, W., Xia, H., Fuh, J. Y. H. & Lu, L. Growth of single-crystal α-MnO2 nanotubes prepared by a hydrothermal route and their electrochemical properties. *J. Power Sources* **193**, 935–938 (2009).

18. Brisse, A. L., Stevens, P., Toussaint, G., Crosnier, O. & Brousse, T. Ni(OH)2 and NiO based composites: Battery type electrode materials for hybrid supercapacitor devices. *Materials* **11**, (2018).

19. Gupta, V., Kawaguchi, T. & Miura, N. Synthesis and electrochemical behavior of nanostructured cauliflower-shape Co–Ni/Co–Ni oxides composites. *Mater. Res. Bull.* **44**, 202–206 (2009).

20. Xu, B. *et al.* Iron oxide-based nanomaterials for supercapacitors. *Nanotechnology* **30**, 204002 (2019).

21. Zhu, J., Tang, S., Xie, H., Dai, Y. & Meng, X. Hierarchically Porous MnO_2 Microspheres Doped with Homogeneously Distributed Fe_3O_4 Nanoparticles for Supercapacitors. *ACS Appl. Mater. Interfaces* **6**, 17637–17646 (2014).

22. O'Neill, L., Johnston, C. & Grant, P. S. Enhancing the supercapacitor behaviour of novel Fe3O4/FeOOH nanowire hybrid electrodes in aqueous electrolytes. *J. Power Sources* **274**, 907–915 (2015).

23. Rakhi, R. B., Chen, W., Cha, D. & Alshareef, H. N. Substrate Dependent Self-Organization of Mesoporous Cobalt Oxide Nanowires with Remarkable Pseudocapacitance. (2012). doi:10.1021/nl300779a

24. Feng, C. *et al.* Sub-3 nm Co_3O_4 Nanofilms with Enhanced Supercapacitor Properties. *ACS Nano* **9**, 1730–1739 (2015).

25. Subramani, K., Kowsik, S. & Sathish, M. Facile and Scalable Ultra-fine Cobalt Oxide/Reduced Graphene Oxide Nanocomposites for High Energy Asymmetric Supercapacitors†. *ChemistrySelect* **1**, 3455–3467 (2016).

26. García-Gómez, A. *et al.* Fabrication of electrochemically reduced graphene oxide/cobalt oxide composite for charge storage electrodes. *J. Electroanal. Chem.* **755**, 151–157 (2015).

27. García-Gómez, A. *et al.* Electrodeposited reduced-graphene oxide/cobalt oxide electrodes for charge storage applications. *Appl. Surf. Sci.* **382**, 34–40 (2016).

28. Pham, T. N. *et al.* Combination-based nanomaterial designs in single and double dimensions for improved electrodes in lithium ion-batteries and faradaic supercapacitors. *J. Energy Chem.* **38**, 119–146 (2019).

29. Tiwari, J. N., Tiwari, R. N. & Kim, K. S. Zero-dimensional, one-dimensional, two-dimensional and three-dimensional nanostructured materials for advanced electrochemical energy devices. *Prog. Mater. Sci.* **57**, 724–803 (2012).

30. Zhan, Y. *et al.* Bestow metal foams with nanostructured surfaces via a convenient electrochemical method for improved device performance. *Nano Res.* **9**, 2364–2371 (2016).

31. Eugénio, S., Demirci, U. B., Silva, T. M., Carmezim, M. J. & Montemor, M. F. Copper-cobalt foams as active and stable catalysts for hydrogen release by hydrolysis of sodium borohydride. *Int. J. Hydrogen Energy* **41**, 8438–8448 (2016).

32. Plowman, B. J., Jones, L. A. & Bhargava, S. K. Building with bubbles: the formation of high surface area honeycomb-like films via hydrogen bubble templated electrodeposition. *Chem. Commun.* **51**, 4331–4346 (2015).

33. Nam, D., Kim, R., Han, D., Kim, J. & Kwon, H. Effects of (NH4)2SO4 and BTA on the nanostructure of copper foam prepared by electrodeposition. *Electrochim. Acta* **56**, 9397–9405 (2011).

34. Popov, K. I., Djokić, S. S., Nikolicć, N. D. & Jović, V. D. *Morphology of electrochemically and chemically deposited metals*. *Morphology of Electrochemically and Chemically Deposited Metals* (2016). doi:10.1007/978-3-319-26073-0

35. Siwek, K. I., Eugénio, S., Silva, T. M. & Fatima Montemor, M. Electrodeposited Manganese Oxide on Tailored 3D Bimetallic Nanofoams for Energy Storage Applications. *Energy Technol.* **7**, 1801139 (2019).

36. Institute, C. History of Cobalt. (2019).

37. Patnaik, P. *Handbook of inorganic chemicals*. (McGraw-Hill, 2003).

38. Antonio De La Peña O'shea, V., De, I., Moreira, P. R., Roldán, A. & Illas, F. Electronic and magnetic structure of bulk cobalt: The , and-phases from density functional theory calculations. *J. Chem. Phys* **133**, 24701 (2010).

39. Tang, N. *et al.* Morphology tuning of porous CoO nanowall towards enhanced electrochemical performance as supercapacitors electrodes. *Catal. Today* 240–245 (2019). doi:10.1016/j.cattod.2018.03.024

40. Wang, C.-B., Lin, H.-K. & Tang, C.-W. Thermal Characterization and Microstructure Change of Cobalt Oxides. *Catal. Letters* **94**, 69–74 (2004).

41. Tompkins, H. G. & Augis, J. A. The oxidation of cobalt in air from room temperature to 467 C. *Oxid. Met.* **16**, 355–369 (1981).

42. Tang, C.-W., Wang, C.-B. & Chien, S.-H. Characterization of cobalt oxides studied by FT-IR, Raman, TPR and TG-MS. *Thermochim. Acta* **473**, 68–73 (2008).

43. Garcia, E. M., Santos, J. S., Pereira, E. C. & Freitas, M. B. J. G. Electrodeposition of cobalt from spent Li-ion battery cathodes by the electrochemistry quartz crystal microbalance technique. *J.*

Power Sources (2008). doi:10.1016/j.jpowsour.2008.07.011

44. Behl, W. K. & Toni, J. E. Anodic oxidation of cobalt in potassium hydroxide electrolytes. *J. Electroanal. Chem. Interfacial Electrochem.* **31**, 63–75 (1971).

45. Upadhyay, K. K., Nguyen, T., Silva, T. M., Carmezim, M. J. & Montemor, M. F. Pseudocapacitive response of hydrothermally grown MoS 2 crumpled nanosheet on carbon fiber. *Mater. Chem. Phys.* (2018). doi:10.1016/j.matchemphys.2018.06.029

46. Gogotsi, Y. & Penner, R. M. Energy Storage in Nanomaterials – Capacitive, Pseudocapacitive, or Battery-like? *ACS Nano* (2018). doi:10.1021/acsnano.8b01914

47. Elgrishi, N. *et al.* A Practical Beginner's Guide to Cyclic Voltammetry. *J. Chem. Educ.* **95**, 197–206 (2018).

48. Adán-Más, A. *et al.* Nickel-cobalt oxide modified with reduced graphene oxide: Performance and degradation for energy storage applications. *J. Power Sources* 12–26 (2019). doi:10.1016/j.jpowsour.2019.02.055